Marine Chemistry 238 (2022) 104066

Contents lists available at ScienceDirect

Marine Chemistry

journal homepage: www.elsevier.com/locate/marchem

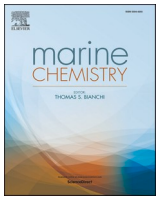

The distribution of Fe across the shelf of the Western Antarctic Peninsula at the start of the phytoplankton growing season

Kyyas Seyitmuhammedov [a,b], Claudine H. Stirling [a,c], Malcolm R. Reid [a,c], Robert van Hale [d,f], Patrick Laan [e], Kevin R. Arrigo [g], Gert van Dijken [g], Anne-Carlijn Alderkamp [g,h], Rob Middag [e,f,*]

[a] Department of Geology, University of Otago, P.O. Box 56, Dunedin, New Zealand
[b] Department of Chemistry, Norwegian University of Science and Technology (NTNU), P.O. Box 8900, 7491 Trondheim, Norway
[c] Centre for Trace Element Analysis, University of Otago, P.O. Box 56, Dunedin, New Zealand
[d] Isotrace, University of Otago, P.O. Box 56, Dunedin, New Zealand
[e] Royal Netherlands Institute for Sea Research (NIOZ), Department of Ocean Systems (OCS), P.O. Box 59, 1790, AB Den Burg, Texel, the Netherlands
[f] Department of Chemistry, University of Otago, PO Box 56, Dunedin, New Zealand
[g] Department of Earth System Science, Stanford University, Stanford, CA 94305, USA
[h] Foothill College, Biology Department, 12345 El Monte Road, Los Altos Hills, CA 94022, USA

ARTICLE INFO

Keywords:
Western Antarctic Peninsula
Iron distribution
Phytoplankton growth season
Iron supply
Iron demand
GEOTRACES

ABSTRACT

The Western Antarctic Peninsula (WAP) is a rapidly changing region with receding sea-ice cover. This region generally has increased phytoplankton productivity on the continental slope with a decrease observed in off-shelf waters located further northward. This study aims to improve the understanding of the distribution of iron (Fe) in this climatically important oceanic region during early sea-ice retreat, as well as the impact of receding ice cover on Fe concentrations and the importance of Fe and its sources at the beginning of the phytoplankton growth season. Five ocean transects were sampled along the Palmer Long Term Ecological Research (Pal-LTER) grid with an additional oceanward extension to access off-shelf waters during the austral spring (October and November) of 2014. High Fe inputs into the entire water column from ice melt as well as from sediments increased dissolved Fe (DFe) and total dissolvable Fe (TDFe) concentrations across the shelf (off-shelf DFe: 0.38 ± 0.30 nmol/L and TDFe: 2.23 ± 2.95 nmol/L versus shelf DFe: 1.54 ± 1.38 nmol/L and TDFe: 19.47 ± 23.82 nmol/L). The combination of meteoric meltwater and shallow sedimentary sources is strongest over the shelf and increased landward towards the WAP. Additionally, a winter sea-ice formation signature was detected in inner shelf waters that appeared to contribute to DFe concentrations. Relatively warm Circumpolar Deep Water (CDW) that flows onto the shelf through troughs is likely modified by non-reductive sedimentary input of Fe into the water column. The increase in Fe concentrations in WAP waters in early spring could trigger enhanced phytoplankton productivity across the shelf, although the highest productivity levels were observed in off-shelf waters, likely related to improved light conditions following receding sea-ice cover. The relatively high productivity levels in WAP off-shelf waters are presumably caused by two factors: (1) supply from below, and (2) the transport of Fe from the shelf to the off-shelf region. However, 80–90% of Fe introduced into shelf waters was removed from the upper water column prior to reaching off-shelf waters, reducing the influence of the coastal Fe source. Low concentrations of DFe (0.24 ± 0.26 nmol/L) in off-shelf waters (upper 100 m) of the WAP coincide with relatively elevated chlorophyll *a* concentrations (0.66 ± 0.56 μg/L), implying that uptake of available DFe had already occurred prior to sampling. Our results imply that the horizontal supply of DFe from the shelf as well as total DFe supply into the surface mixed layer might not be sufficiently high to support productivity in the off-shelf waters of the WAP, underlining the development of an Fe deficit early in the growth season.

* Corresponding author.
E-mail address: rob.middag@nioz.nl (R. Middag).

https://doi.org/10.1016/j.marchem.2021.104066
Received 8 December 2020; Received in revised form 10 November 2021; Accepted 17 November 2021
Available online 26 November 2021

1. Introduction

The Western Antarctic Peninsula (WAP) is one of the most intensively studied regions of Antarctica due to the Palmer Long Term Ecological Research (Pal-LTER) program that began in 1990 (Ducklow et al., 2013; Steinberg et al., 2012). This region is known to have high primary productivity (Vernet et al., 2008) in some coastal regions, known as biological 'hotspots' (Sherrell et al., 2018), featuring abundant organisms at all trophic levels (Kavanaugh et al., 2015; Schofield et al., 2013). The regional productivity is influenced by the extent, duration, and seasonality of sea-ice and glacial discharge (Ducklow et al., 2013). Marine primary productivity results in carbon drawdown from the atmosphere with subsequent transfer of organic matter to the deep ocean via the biological pump, establishing the Southern Ocean as a potential sequestration region for carbon dioxide (CO_2) (Brown et al., 2019; Henley et al., 2020; Martin, 1990; Yang et al., 2021). The continental shelf of Antarctica accounts for ~10% of Southern Ocean productivity with the remaining ~90% occurring in off-shelf and open ocean waters (Arrigo et al., 2008), although the productivity per unit of surface area is much larger in shelf regions. The Antarctic Peninsula experienced rapid warming in the second half of the 20th century (Marshall et al., 2006), resulting in surface melt of glaciers (Barrand et al., 2013; Holland et al., 2015; Kunz et al., 2012; Pritchard and Vaughan, 2007). More importantly, intruding warm deep waters along the WAP promote basal melt that further decreases ice sheet cover (Cook et al., 2016).

Phytoplankton require major nutrients and micronutrients, including trace metals, to grow. A critically important micronutrient is iron (Fe), which acts as a primary electron contributor and acceptor during photosynthesis and as a cofactor in enzymes in nitrate assimilation (Raven, 1988). Additionally, due to the different requirements of different species, dissolved iron (DFe) concentrations in seawater can control the primary production and the species composition of the phytoplankton community (Coale et al., 1996). This is especially the case in 'high-nutrient, low-chlorophyll (HNLC)' waters, such as those of the Southern Ocean south of the Polar Front (de Baar, 2005; Henley et al., 2020; Tagliabue et al., 2017), which have elevated surface water macronutrient concentrations but relatively low levels of primary production due to the combination of low levels of light and biologically important trace metals, notably Fe (Moore, 2013). It has been suggested previously that Fe played a crucial role in maintaining low levels of atmospheric CO_2 during the Last Glacial Maximum by stimulating high marine productivity (Martin, 1990), making Fe a crucial player in global climate.

Dissolved Fe is known to have a hybrid type distribution in the oceans that is dominated by microbial uptake, recycling and scavenging processes, leading to generally low surface concentrations (Bruland et al., 2014). Input processes of dissolved and particulate Fe in the Southern Ocean include a combination of: (1) atmospheric deposition (Gao et al., 2020; Gao et al., 2013; Tagliabue et al., 2009; Winton et al., 2015), (2) hydrothermal input (Tagliabue et al., 2010), (3) meltwater from sea-ice (Lannuzel et al., 2011; Lannuzel et al., 2007, 2010), glaciers and icebergs (Annett et al., 2015; Bown et al., 2017; Lin et al., 2011; Raiswell et al., 2016; Raiswell et al., 2008), (4) sea-ice formation (Schallenberg et al., 2016), (5) sedimentary input from the resuspension of sedimentary particles (de Jong, 2012), (6) dissolution from sediments and/or pore waters (de Jong, 2012; Hatta et al., 2013; Measures et al., 2013), (7) mixing processes such as advection and diffusion from distant and/or nearby sources (De Jong et al., 2015; Tagliabue et al., 2014) and (8) buoyancy-driven circulation due to melting ice via 'the meltwater pump' that results in the horizontal and vertical supply of Fe derived from both the sediments as well as glacial melt (St-Laurent et al., 2017; St-Laurent et al., 2019; Twelves et al., 2021). The latter process, where glacial melt induced by warm intruding water leads to upwelling, has been shown to be especially important for delivering Fe to surface waters in some Antarctic shelf seas (e.g. St-Laurent et al., 2017). Removal processes include (1) oxidative precipitation (Millero et al., 1987), (2) adsorptive scavenging (Measures et al., 2013), and (3) phytoplankton uptake (Bown et al., 2017).

Previous studies have based their findings of the processes controlling the distribution of Fe in WAP waters on surface Fe concentrations (~2 m depth) across the shelf (Annett et al., 2017) and a limited area in the inner-shelf (Sherrell et al., 2018) during the austral summer. These investigations provided important initial constraints on some of the major processes influencing Fe distributions in WAP waters, as well as in other shelf regions of Antarctica. The Fe concentrations in WAP waters have been suggested to be controlled by inputs from meltwater, (shallow) sedimentary sources across the shelf, and horizontal transport of CDW waters across the shelf break and advection of coastal waters from the inner shelf regions (Annett et al., 2017; Sherrell et al., 2018). However, summer Fe concentrations are very much depleted, making it harder to assess the impact of other essential processes on Fe distributions in the surface layer. Our study builds upon these earlier findings by reporting Fe distributions and concentrations in waters adjacent to the WAP based on depth profiles across the WAP shelf, from near the coast to the off-shelf region. Moreover, this study reports Fe distributions for the beginning of the phytoplankton growth season (early austral spring), allowing the Fe stock at the beginning of the growth season, when sea-ice is retreating, to be determined. In addition, Mn values are reported and used here to help identify sedimentary sources of Fe, while the processes affecting Mn distributions and those of other essential trace metals will be discussed elsewhere (in preparation). Our study aims to differentiate and characterize the sources of Fe in the shelf region and to assess the influence of shelf waters as a potential Fe source to the off-shelf region.

2. Methods

2.1. Study region and hydrography

The study region comprises the Pal-LTER grid with an ocean-ward extension (Fig. 1A). This grid is located on the western side of the Antarctic Peninsula. The Pal-LTER sampling transects are arranged perpendicular to the peninsula at 100 km intervals along lines 200, 300, 400, 600 and 700, extending from the coastline to 200 km offshore (Fig. 1A). In this study, the lines were extended by an additional 200 km offshore from the shelf break to include off-shelf samples as previously described (Arrigo et al., 2017).

The offshore region of the study area is characterized by cold, fresh Antarctic Surface Water (AASW) underlain by warmer Upper Circumpolar Deep Water (UCDW) that is characterized by an oxygen minimum, and Lower Circumpolar Deep Water (LCDW) that is slightly colder but more saline than UCDW (Fig. 1 B–C, S1). The AASW is defined as water with a potential temperature < -1.4 °C and salinity <34, while UCDW consists of water with a potential temperature > 1.5 °C and salinity between 34.4 and 34.7, and LCDW is defined as water with a potential temperature between 1.0 and 1.5 °C and salinity >34.7 following earlier definitions (Arrigo et al., 2017).

The waters adjacent to the WAP contain the Polar Front (PF), southern ACC Front (SACCF) and the southern boundary of the ACC (SBACC). The Polar Front is located north of the study area, whereas the SACCF and SBACC are located within the study region (Fig. 1A). Stations between these fronts have similar upper water column characteristics, whereas stations separated by the fronts have different characteristics, becoming warmer, fresher and less dense towards the off-shelf. The CDW water from the ACC intrudes across the shelf through troughs, with eddy events, flooding over the shelf (Moffat and Meredith, 2018).

The study region also contains two clockwise gyres (Hofmann et al., 1996), one near Anvers and Brabant Islands and the other near Adelaide Island. These two gyres are the result of a northeast flowing current along the shelf edge following the ACC route and the southwest flowing Antarctic Peninsula Coastal Current (APCC) (Moffat et al., 2008). The APCC is defined as a strong, narrow current near the coast formed by

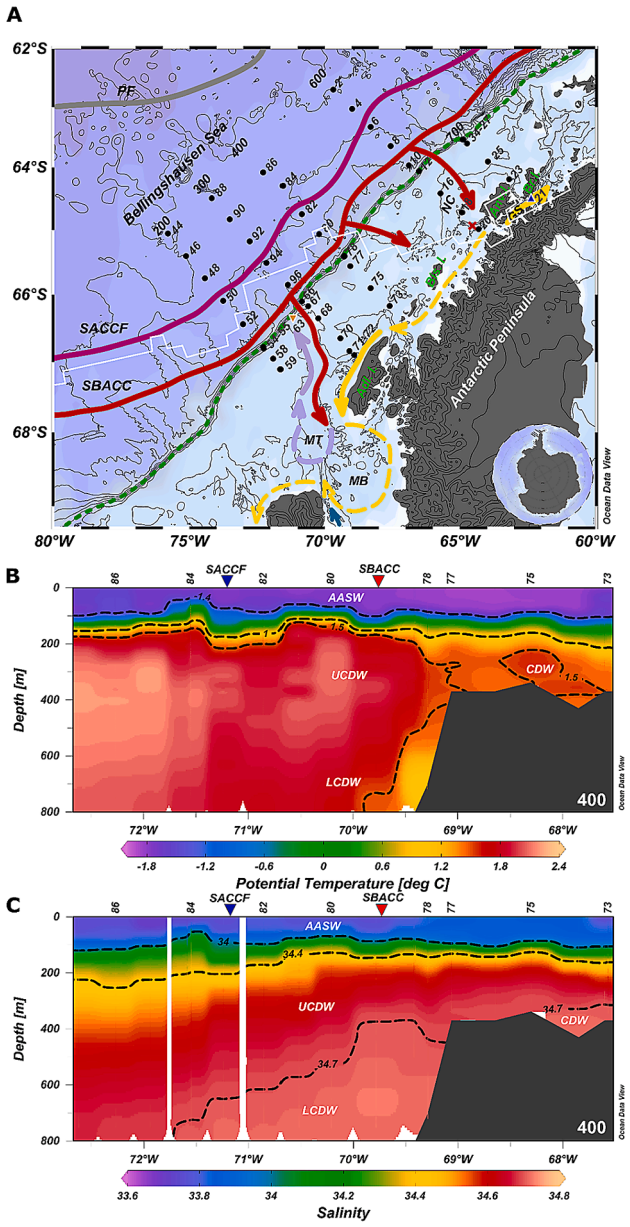

Fig. 1. A. Map of the Western Antarctic Peninsula (WAP) study region with sampling lines 200 to 700 and station numbers indicated next to the station symbols. **1B.** Distribution of potential temperature in color scale along sampling line 400 with water masses indicated with black dashed lines and the location of fronts indicated by a blue triangle for SACCF and by a red triangle for SBACC. **1C.** Distribution of salinity in color scale along sampling line 400 with AASW, UCDW, LCDW indicated with black dashed lines and the location of fronts indicated by a blue triangle for SACCF and by a red triangle for SBACC. Abbreviations: Adl. I. – Adelaide island; Anv .I. – Anvers Island; AASW – Antarctic Surface Water, UCDW – Upper Circumpolar Deep Water, LCDW – Lower Circumpolar Deep Water, Bis. I. – Biscoes Islands; Br. I. – Brabant Island; GS – Gerlache Strait; MB – Marguerite Bay; MT- Marguerite Trough; NC – Northern Canyon; PF – Polar Front; SACCF – Southern Antarctic Circumpolar Current Front; SBACC – Southern Boundary of Antarctic Circumpolar Current. Arrows: Yellow arrow – Antarctic Polar Coastal Current (APCC: solid – confirmed route, and dashed – suspected route); Red arrows – intrusion of CDW; Purple arrow – outflow current (solid – confirmed current, and dashed - suspected current); Cyan arrow – suspected George VI Ice Shelf input; Red cross symbol – Palmer Deep Trough; White-blue triangle symbol – station 21; White-orange triangle symbol – station 63; Dashed green line – 500 m isobaths shelf break; White solid line – sea-ice extent during the sampling period. Adapted from Moffat and Meredith, 2018. (For interpretation of the references to color in this figure legend, the reader is referred to the web version of this article.)

freshwater discharge and downwelling-favorable winds (Moffat et al., 2008). This current flows southwest from Anvers Island, along Biscoe and Adelaide Islands into Marguerite Bay, south of Adelaide Island, and northeast between the Antarctic Peninsula and Anvers and Brabant Islands (Moffat et al., 2008; Moffat and Meredith, 2018; Savidge and Amft, 2009) (Fig. 1A). The APCC current can reach depths of 100–150 m and be up to 20 km wide (Moffat and Owens, 2008; Moffat and Meredith, 2018; Savidge and Amft, 2009).

Samples were obtained in early spring (October and November 2014) while melting of the seasonal sea-ice was ongoing. The mean open water area was ~170,000 km^2 in August/September and increased to ~332,000 km^2 in December/January (Arrigo et al., 2017). The peak in ice-free water was reached one month earlier (December) in off-shelf waters than in shelf waters (January) (Arrigo et al., 2017). Therefore, the peak in ice-free water occurred after the sampling period, but the extent of ice-free water was already larger in the off-shelf region and ice cover increased shoreward from the shelf break towards the continent (Arrigo et al., 2017). The southern zone of the sampling region (lines 200 and 300) had the highest sea-ice cover, approaching 100%, and in the northernmost part of the sampling region (line 700) cover was only 30% during the time of sampling (Arrigo et al., 2017).

2.2. Sample collection

Seawater samples were collected with a trace-metal clean CTD rosette equipped with GO-FLO bottles until the rosette was lost due to failure of the Kevlar cable after completing line 600 and half of line 700. Thereafter, seawater samples were collected with GO-FLO bottles deployed on the remaining Kevlar cable and triggered manually with messengers. Samples for trace metal concentration analysis, including both dissolved metals (DM) and total dissolvable metals (TDM), were collected into 60 mL LDPE (Nalgene) bottles that were rigorously acid-cleaned prior to the expedition following GEOTRACES protocols (Gerringa et al., 2020). Samples for DM analysis were filtered through a 0.2 μm filter (Sartobran 300, Sartorius) directly from the GO-FLO bottles under 0.5 bar nitrogen gas overpressure, while TDM samples were unfiltered. All samples were then acidified to 0.024 M HCl (pH ~ 1.8) with ultra-pure HCl (Optima grade Fisher Scientific). All samples were collected under clean conditions inside a trace metal clean van equipped with trace metal clean laminar flow benches. The labile particulate fraction of a metal (lpM) was calculated by subtracting DM from TDM concentrations.

Samples for $\delta^{18}O$ analysis were collected into 25 mL glass vials and stored at room temperature. Samples for chlorophyll *a* analysis were collected as described previously (Arrigo et al., 2017). Samples for major nutrients (nitrate and phosphate) were analyzed simultaneously with a discrete autoanalyzer TRAACS 800 (Technicon) in the shore-based laboratory of the Royal Netherlands Institute for Sea Research (NIOZ), the Netherlands.

2.3. Sample analyses

2.3.1. Multi-element concentration analysis

All filtered samples and some unfiltered samples were analyzed at NIOZ, while the remaining unfiltered samples were analyzed at the University of Otago. Pre-concentration of seawater samples was done using a seaFAST pico (ESI, USA) system equipped with Nobias-chelate PA1 chelating resin (Hitachi High-technologies, Japan) after UV-oxidation as detailed by Gerringa et al. (2020). Samples were analyzed using a Thermo Element2 Sector-Field ICP-MS (SF ICP-MS) at NIOZ and a Nu Attom SF ICP-MS at the University of Otago. Using a microFAST system (ESI), 250 μL of sample was introduced into the ICP-MS via an ESI-PC3 Peltier cooled spray chamber (4 °C) with a micro-FAST PFA nebulizer at a constant rate of 35 μL min^{-1}. The preconcentration recoveries were verified in every analytical run by comparing the slope of the seawater calibration curve (multi-element standard added to

the seawater sample from the surface waters of South Pacific Ocean) and the eluent calibration curve (multi-element standard added directly to the elution acid) after Biller and Bruland (2012). Recoveries were > 98% for both Fe and Mn.

Blank contributions from sample handling, pre-concentration and analysis were determined by analyzing acidified high-purity water (~1.8 pH) (Milli-Q Element purification unit, Millipore Ltd., USA) as a sample. The determined blank values for both laboratories were comparable (Table 1).

The accuracy and precision of the measurements was determined by measuring the reference sample GEOTRACES South Pacific (GSP) as well as in-house reference seawater samples, notably a surface seawater sample (Munida 0) for low concentration samples, as well as North Atlantic Deep Water (NADW) and surface seawater spiked with known concentrations of trace metals (Munida +) for medium to high concentration samples (Table 1). Additionally, the NASS 7 certified reference material was analyzed and the concentrations of two stations (72 and 73) were determined in both laboratories (NIOZ and University of Otago) for intercomparison between the institutes, which showed good agreement within the magnitude of their analytical uncertainties (Table 1).

2.3.2. $\delta^{18}O$ analysis

Samples comprising 0.5 mL were analyzed at the Isotrace Laboratory, University of Otago by equilibrating with 12 mL of 0.3% CO_2 in helium on a Thermo (Bremen) GasBench preparation unit for 18 h at 25.0 ± 0.01 °C. Ten repeat injections of the equilibrated gas were measured with a Thermo Advantage isotope ratio mass spectrometer (IRMS) in continuous-flow mode. The 10 raw results were filtered by removal of values more than 1 standard deviation from the average. The filtered average was corrected to the international VSMOW-SLAP isotope scale using a three-point calibration provided by three laboratory standards analyzed before and after every batch of 84 samples. In addition, a control sample chosen to be similar to the samples being measured was analyzed at every 12th position to correct for instrumental drift. The instrumental drift correction, if applied, was calculated from a linear regression of the control sample results against time. Consensus values for the laboratory standards have been obtained from six-year internal laboratory calibration records against primary reference materials, VSMOW, GISP and SLAP, an external six member interlaboratory comparison exercise, and by back-calculation from the ~170 member IAEA interlaboratory comparison exercise, WICO2012. The laboratory standards and their consensus values are as follows: ICE ($\delta^{18}O_{VSMOW} = -32.097 \pm 0.075$ milliurey (mUr = 1‰)), TAP ($\delta^{18}O_{VSMOW} = -11.432 \pm 0.038$ mUr), and SEA ($\delta^{18}O_{VSMOW} = -0.029 \pm 0.036$ mUr).

The proportions of meteoric and seawater were calculated using the method of (Meredith et al., 2013). Three-component mass balance equations for meteoric water, ice melt and CDW were solved using the inverse matrix technique.

$$\begin{aligned} f_{sim} + f_{met} + f_{CDW} &= 1 \\ S_{sim} \times f_{sim} + S_{met} \times f_{met} + S_{CDW} \times f_{CDW} &= S \\ \delta_{sim} \times f_{sim} + \delta_{met} \times f_{met} + \delta_{CDW} \times f_{CDW} &= \delta \end{aligned} \quad (1)$$

where f_{sim}, f_{met}, and f_{CDW} are the fractions of sea ice melt, meteoric water, and CDW, respectively; S_{sim}, S_{met}, and S_{CDW} are the respective salinities of the pure components of sea ice melt, meteoric water, and CDW; and δ_{sim}, δ_{met}, and δ_{CDW} are their corresponding $\delta^{18}O$ values. The quantities S and δ are the measured values of salinity and $\delta^{18}O$ in each water sample for which the sea ice and meteoric freshwater contributions are being derived. Following the Meredith et al. (2013) study in the LTER grid region, the endmembers are assigned values of 34.73 and + 0.1 mUr for the salinity and $\delta^{18}O$ of the CDW endmember, respectively. Sea ice melt is assigned corresponding values of 7 and + 2.1 mUr, and meteoric water is assigned values of 0 and − 16 mUr.

2.4. Dissolved iron supply calculations

2.4.1. Horizontal diffusive supply of dissolved iron

The horizontal supply in the surface mixed layer (SML) and below the SML from the peninsula towards the off-shelf region was estimated for each sampling line using a one-dimensional advection/diffusion model simplified from de Jong, 2012 by only estimating the horizontal diffusive supply (J_{hs}).

$$J_{hs} = -K_h \times \left(\frac{\partial^2 [DFe]}{\partial x^2} \right) \quad (2)$$

Similar horizontal supplies via diffusion only were estimated in other parts of the Southern Ocean as well (Bucciarelli et al., 2001; Gerringa et al., 2015; Johnson et al., 1997; Planquette et al., 2007). The simplified one-dimensional advection/diffusion model equation uses only horizontal eddy diffusive flux divergence (μmol m^{-3} s^{-1}) in Eq. (2), which is

Table 1
Blanks, limits of detection and analytical performance of seawater trace metal consensus samples, reference materials and intercomparison stations.

Blank								
Elements	NIOZ	n	U. Otago	n				
Mn (nmol/L)	0.003 ± 0.001	24	0.002 ± 0.001	18				
Fe (nmol/L)	0.05 ± 0.02	21	0.03 ± 0.007	17				
Limit of detection (3xSD)								
Mn (nmol/L)	0,004		0,004					
Fe (nmol/L)	0,05		0,02					
NIOZ								
GEOTRACES South Pacific (GSP)				**SAFe D1**[a]			**NADW**	
Elements	Determined	n	Consensus	Determined	n	Consensus	Determined	n
Mn (nmol/L)	0.787 ± 0.011	14	0.778 ± 0.034	0.421 ± 0.006	3		0.443 ± 0.005	17
Fe (nmol/L)	0.150 ± 0.009	13	0.155 ± 0.045	0.722 ± 0.008	3	0.69 ± 0.04	0.597 ± 0.021	17
U. Otago								
SAFe D1					**Munida 0**		**Munida +**	
Elements	Determined	n	Consensus	Elements	Determined	n	Determined	n
Mn (nmol/L)	0.417 ± 0.009	6		Mn (nmol/L)	0.121 ± 0.005	20	0.841 ± 0.019	19
Fe (nmol/L)	0.729 ± 0.018	6	0.69 ± 0.04	Fe (nmol/L)	0.037 ± 0.022	19	0.774 ± 0.026	19
NASS7				**Station 72**				
Elements	Determined	n	Certified	Elements	NIOZ	n	U. Otago	n
Mn (μg/L)	0.72 ± 0.02	4	0.75 ± 0.06	Mn (nmol/L)	0.87 ± 0.12	8	0.89 ± 0.10	7
Fe (μg/L)	0.336 ± 0.011	4	0.351 ± 0.026	Fe (nmol/L)	0.91 ± 0.62	8	0.93 ± 0.56	7
							Staion 73	
				Mn (nmol/L)	2.34 ± 1.08	6	2.40 ± 1.12	6
				Fe (nmol/L)	2.00 ± 0.53	6	2.12 ± 0.55	6

[a] SAFe consensus values were converted to molar units using density value of 1.025 kg/L.

the product of the horizontal eddy diffusivity (K_h, $m^2\ s^{-1}$) and the curvature of the horizontal DFe gradient ($\frac{\partial^2[DFe]}{\partial x^2}$, μmol m^{-5}), as input parameters (de Jong, 2012). The assumed off-shelf value of 0.05 nmol/ L was subtracted from the depth-averaged DFe concentration for flux estimates in and below the SML. The concentrations versus distance from the shore for each sampling line were best fitted with a power function. The SML depth was defined as the depth at which the potential density was 0.1 kg/m^{-3} greater than at the surface (Dong et al., 2008) and fluxes below the SML were calculated between the SML and the previously defined permanent pycnocline at a depth of 160 m (Couto et al., 2017).

There is no defined advective velocity from the peninsula towards the off-shelf area for the study region as the main currents flow along the shelf (Fig. 1). Therefore, in this study, horizontal diffusion is used as a plausible mechanism for Fe to be transported from the shelf into the ACC. The horizontal diffusivity (K_h) can be estimated by scale length using the empirical relationship $K_h = 0.0103 \times l^{1.15}$ (de Jong, 2012; Okubo, 1971). The scale length (l) is the distance at which the initial DFe concentration has decreased by 95% (Okubo, 1971) which was estimated as three times the distance by which DFe decreases by $1/e$ of its initial concentration after Johnson et al. (1997). Horizontal diffusivities in the SML along lines 700 and 300 were estimated to be between 360 and 650 $m^2\ s^{-1}$. Additionally, horizontal diffusivities were estimated between the SML and the permanent pycnocline resulting in values between 386 and 766 $m^2\ s^{-1}$. Horizontal and vertical supplies were estimated for all sampling lines except line 200 as the shelf region of this transect was not sampled. Couto et al. (2017) also pointed out that an anomalously high horizontal diffusivity of 1600 $m^2\ s^{-1}$ in the WAP region has been determined by Klinck et al. (2004), but reported this value as unrealistic and used previously reported values of 37 and 200 $m^2\ s^{-1}$ for the shelf region (Klinck, 1998; Smith et al., 1999). For consistency among the transects, 548 ± 135 $m^2\ s^{-1}$ (mean ± 1 SD) in the SML and 588 ± 160 $m^2\ s^{-1}$ (mean ± 1 SD) below the SML, the means of the horizontal diffusivities estimated in this study, were instead used to estimate a maximum horizontal supply for each depth interval, and 37 ± 3 $m^2\ s^{-1}$ was used to estimate a minimum horizontal supply both in and below the SML. These values were used throughout rather than using a different diffusivity for each transect to minimize the influence of spatial/temporal differences.

2.4.2. Vertical advective and diffusive supply of DFe

Vertical advection is the product of the upwelling velocity due to Ekman suction (upwelling) and the DFe concentration below the base of the SML. The vertical diffusive supply is the product of the vertical eddy diffusivity and the slope of the DFe depth gradient between the lowest DFe concentration in the SML and below the SML. Grotov et al. (1998) reported vertical advection velocity (upwelling) in the Bellingshausen Sea of between 6.34×10^{-7} and 7.93×10^{-7} m s^{-1}. Furthermore, a large range has been reported for vertical diffusivity (K_z) in WAP waters with a minimum value of below 1×10^{-5} $m^2\ s^{-1}$ and an upper value of 1×10^{-4} $m^2\ s^{-1}$ (Couto et al., 2017; Hoppema et al., 2002; Howard et al., 2004; Klinck, 1998; Martinson and McKee, 2012; Martinson et al., 2008; Moffat and Meredith, 2018). Therefore, we opted to use both the upper and lower estimates of advection and diffusivity to obtain an upper and lower estimate of vertical DFe supply.

3. Results

3.1. Iron

Generally, the concentration of DFe and TDFe increased towards the continent and with increasing depth. The highest concentrations were measured over the shelf and the lowest concentrations were obtained in the off-shelf SML (Fig. 2A–B). Most stations over the shelf had high concentrations in the SML and subsurface waters (below the SML) (Fig. 3). Additionally, DFe and TDFe concentrations were elevated with

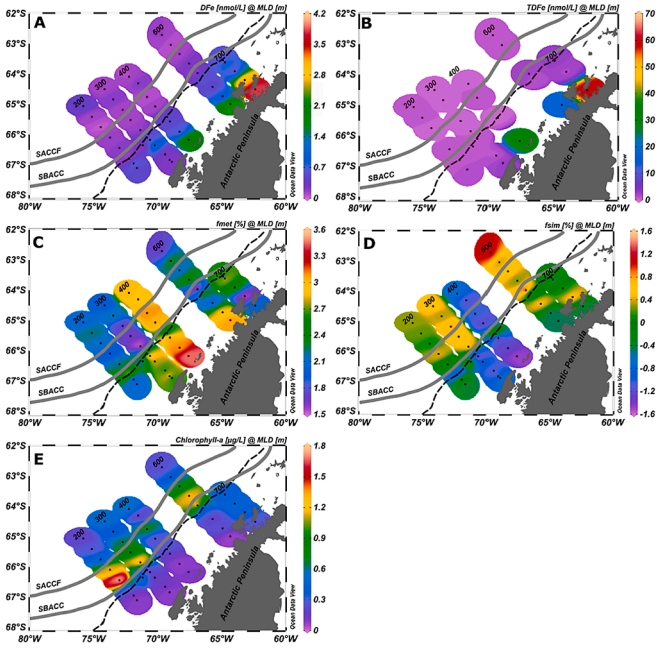

Fig. 2. Color scale surface distributions of depth-averaged Fe, meltwater based on $\delta^{18}O$, and chlorophyll *a* in the SML showing the highest concentrations between the SACCF and SBACC fronts. SML distribution of **A.** Dissolved Fe (DFe); **B.** Total dissolvable Fe (TDFe); **C.** Sea-ice meltwater fraction (sim); **D.** Meteoric meltwater fraction (met); **E.** Chlorophyll *a*. Dashed black line – 500 m isobath shelf break. Abbreviations as in Fig. 1.

depth towards the seafloor (Fig. 3). The Fe concentrations over the shelf ranged from 0.18–8.10 nmol/L (mean 1.54 ± 1.38 nmol/L, median 1.07 nmol/L, n = 175) for DFe and 0.40–102.34 nmol/L (mean 19.47 ± 23.82 nmol/L, median 7.95 nmol/L, n = 84) for TDFe. Off-shelf Fe concentrations were comparatively low, with values of <0.05–1.44 nmol/L (mean 0.38 ± 0.30 nmol/L, median 0.29 nmol/L, n = 179) for DFe and 0.16–17.80 nmol/L (mean 2.23 ± 2.95 nmol/L, median 1.28 nmol/L, n = 121) for TDFe.

The highest SML DFe and TDFe concentrations along each sampling line occurred at the stations closest to the continent for sampling lines 700 (station 23), 600 (station 20) and 400 (station 73; Table 2; Fig. 3A–F). The remaining sampling lines 300 and 200 had elevated concentrations of Fe (DFe: 0.31–1.84 nmol/L; TDFe: 0.98–2.06 nmol/L; Fig. 3G–J) at mid-shelf and shelf break stations. However, for sampling line 300, stations close to the peninsula had lower DFe concentrations with only slightly elevated TDFe concentrations (DFe: 0.21–0.52 nmol/ L; TDFe: 0.94–8.96 nmol/L; Fig. 3G–H).

Relatively high DFe and TDFe concentrations were also found near the seafloor (~50 m above bottom depth) across the continental shelf for all sampling lines. In particular, sampling lines 200 and 300 had significantly higher Fe concentrations near the seafloor (mean DFe: 1.89 ± 1.30 nmol/L; mean TDFe: 43.62 ± 30.98 nmol/L) than surface concentrations (mean DFe in MLD: 0.62 ± 0.47 nmol/L; mean TDFe in SML: 2.05 ± 2.11 nmol/L). The highest bottom water concentrations were observed along sampling line 300 (stations 70 and 71; Fig. 3G–H). In contrast, along sampling lines 600 and 400, comparatively high DFe and TDFe was observed in the SML (stations 20 and 73; Fig. 3C–F), although bottom water Fe was still elevated (DFe = 2.49 nmol/L and TDFe = 32.14 nmol/L at station 20; DFe = 1.18 nmol/L and TDFe = 17.27 nmol/ L at station 73) relative to off-shelf subsurface and deep waters (>160 m DFe: 0.52 ± 0.27 nmol/L; TDFe: 3.51 ± 4.09 nmol/L). Furthermore, close to the continent, sampling line 700 had similar DFe in the SML and near the seafloor (depth-averaged DFe in SML = 3.05 nmol/L; DFe near seafloor = 3.40 nmol/L at station 23; Fig. 3A).

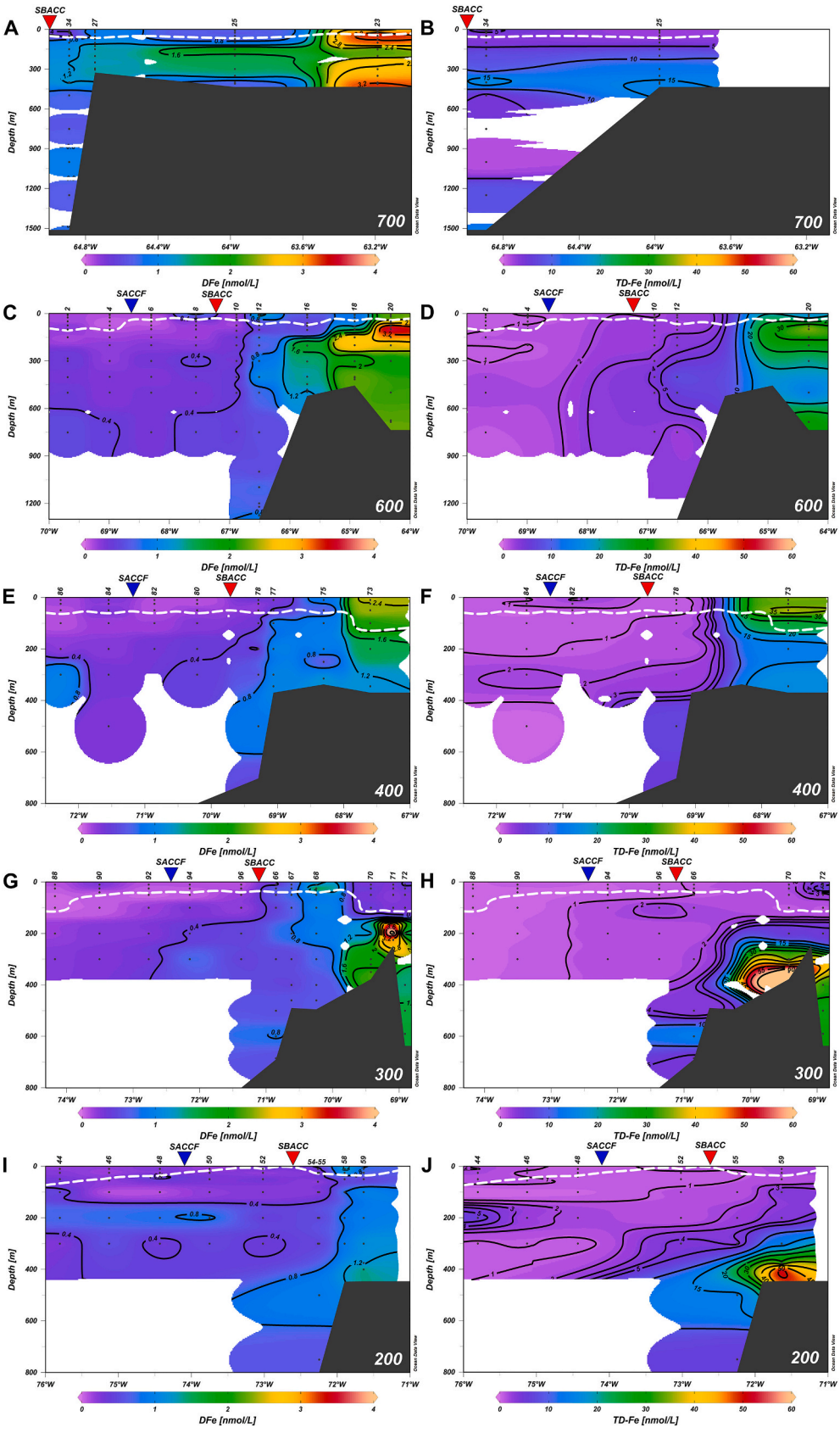

Fig. 3. Distribution of dissolved (DFe) and total dissolvable Fe (TDFe) in color scale along sampling lines 700 (A and B), 600 (C and D), 400 (E and F), 300 (G and H) and 200 (I and J). Please note the color scale is different for DFe and TDFe. Surface mixed layer depth is indicated by a white dashed line and abbreviations as in Fig. 1.

Table 2
Depth-averaged dissolved and total-dissolvable Fe concentrations in and below the surface mixed layer.

Transect	Station	Bottom Depth	SML	$DFe_{\int SML}$	$TDFe_{\int SML}$	$DFe_{\int PP}$	$TDFe_{\int PP}$
#	#	m	m	nmol/L	nmol/L	nmol/L	nmol/L
			Shelf region				
700	21	689	56	3.81	59.18	3.59	42.49
700	23	434	47	3.06		2.86	
700	25	435	82	0.62	1.84	1.35	1.84
700	27	326	75	0.99		1.23	
700	34	1512	76	0.41	2.84	1.01	1.87
600	20	736	62	2.28	17.26	3.32	37.59
600	18	455	68	0.81		1.96	
600	16	521	85	0.49		0.75	
400	73	370	101	2.06	29.66	1.92	20.91
400	75	338	78	0.65		0.94	
400	77	370	91	0.47		1.00	
400	78	703	79	0.17	0.54	0.25	1.23
300	72	637	106	0.26	2.77	0.55	2.22
300	71	248	108	0.19		1.81	
300	70	378	100	0.29	1.13	0.57	2.17
300	68	495	74	1.03		1.00	
300	67	490	85	0.66		0.68	
300	66	690	76	0.46	1.02	0.36	1.55
300	63	705	85	0.21	1.20	0.28	1.31
200	59	446	75	0.45	1.50	0.96	3.57
200	58	448	87	0.84		0.87	
200	55	1015	95	0.15	0.66	0.18	1.24
200	54	1660	95	0.12		0.22	
			Off-shelf region				
600	12	1530	78	0.68	1.74	0.50	3.46
600	10	3073	69	0.10	2.18	0.19	3.76
600	8	3387	74	0.24		0.11	
600	6	3592	75	0.15		0.08	
600	4	3801	106	0.08	0.83	0.08	0.25
600	2	4017	127	0.15	0.77	0.09	1.23
400	80	2500	72	0.12		0.21	
400	82	3431	89	0.08	0.88	0.14	0.65
400	84	3660	72	0.20	0.58	0.01	0.11
400	86	3710	100	0.09		0.08	
300	96	3100	50	0.16	0.50	0.17	2.16
300	94	3564	86	0.13	0.59	0.27	1.34
300	92	3645	93	0.10		0.12	
300	90	3210	108	0.21	0.30	0.19	0.32
300	88	3849	119	0.11	0.20	0.10	0.20
200	52	3692	48	0.19	0.69	0.22	1.00
200	50	3650	56	0.15		0.30	
200	48	3880	86	0.06	0.41	0.41	0.83
200	46	4019	101	0.18	0.80	0.44	1.21
200	44	3990	136	0.37	1.21	0.55	3.25
Average	**Shelf region**			**0.89**	**9.97**	**1.20**	**9.83**
	Off-shelf region			**0.18**	**0.84**	**0.21**	**1.41**
	Decrease			**80%**	**92%**	**82%**	**86%**

3.2. Manganese

Generally, the concentrations of DMn and TDMn increased towards the continent and with increasing depth. The Mn concentrations over the shelf ranged from 0.20–4.14 nmol/L (mean 1.31 ± 0.87 nmol/L, median 1.04 nmol/L, $n = 178$) for DMn and 0.30–5.47 nmol/L (mean 1.84 ± 1.38 nmol/L, median 1.07 nmol/L, $n = 84$) for TDMn. The off-shelf Mn content was relatively low, ranging from 0.08–2.96 nmol/L (mean 0.32 ± 0.34 nmol/L, median 0.24 nmol/L, $n = 189$) for DMn and 0.17–1.76 nmol/L (mean 0.44 ± 0.33 nmol/L, median 0.29 nmol/L, $n = 121$) for TDMn.

3.3. Oxygen isotopes ($\delta^{18}O$)

Oxygen isotope ratios showed high meltwater input along most sampling lines. The meltwater contribution is a combination of meteoric (glacial melt and precipitation) and/or sea-ice melt. The meteoric fraction increased towards the peninsula and the sea-ice melt contribution increased towards the off-shelf (Fig. 2C–D, S3). A broad tongue, centering along the sampling line 400, of particularly light water (−0.6 to −0.3‰) extended out from land for the full length of the sampling line. The inshore stations of the sampling lines either side (lines 300 and 600) of line 400 also showed low $\delta^{18}O$ in the SML, especially so along line 300. The highest meteoric meltwater input to the sampling region occurred along sampling line 400, notably in inner shelf waters (station 73), with the meltwater fraction decreasing off-shelf (Fig. 2D, S3E). The elevated meteoric meltwater fraction was accompanied by deeper mixing (Fig. S2) along this line where the meteoric meltwater fraction was also elevated at depth (Fig. S3E). The lowest meteoric meltwater fraction was estimated for the inner shelf waters of sampling line 700 (station 23) and Gerlache Strait (station 21) (Fig. 2D, S3A). The second highest meteoric influence was estimated for the middle and inner shelf waters of sampling line 300 (Fig. 2D, S3G). The highest positive sea-ice meltwater input was calculated for off-shelf waters and additionally the influence of sea-ice melt was inferred for shelf waters of sampling line 600 (station 16) and inner shelf waters of sampling line 700 (station 23) (Fig. 2C, S3B, S3D). The shelf and off-shelf waters of sampling line 400, as well as the shelf waters of line 300, had a negative sea-ice meltwater

fraction, which is the signature of sea-ice formation (Fig. 2C, S3F, S3H), as was observed in other regions of Antarctic shelf seas (e.g. Meredith et al., 2008; Meredith et al., 2017; Meredith et al., 2013; Randall-Goodwin et al., 2015).

Broadly, there was a similar distribution for meteoric meltwater and Fe in the SML. However, there was no overall correlation between either DFe and TDFe and the sea-ice or meteoric melt fractions in the SML for the whole sampling grid. There was, however, a positive correlation between DFe and the meltwater fractions when assessing the individual sampling transects (Table 3), except for sampling line 200, most likely due to a dearth of samples because of the continuous ice cover preventing sampling towards the continent. However, there was also a positive correlation between DFe and the distance from the coast for the same sampling lines except for line 300 (Table 3). Elevated DFe can be observed in the middle of this transect (station 68) that aligns with observed high-density water in the SML (Fig. S2D). A negative relationship between DFe and the sea-ice fraction was observed for sampling lines 700, 600, 400 and 300 (Table 3).

3.4. Chlorophyll a

Chlorophyll *a* concentrations reported previously by Arrigo et al. (2017) are used for the interpretation of the distribution of Fe. The depth-averaged chlorophyll *a* in the SML were elevated between the SACCF and SBACC fronts with the highest concentrations occurring in the southwest of the study region (stations 50 and 52) (Fig. 2E).

4. Discussion

4.1. Historical Fe data in the Pal-LTER grid of the western Antarctic Peninsula

Previously determined near-surface (~2 m depth) DFe for the Pal-LTER sampling grid during the austral summers of 2010, 2011 and 2012 (Annett et al., 2017) showed a larger range in dissolved concentrations than the present study carried out in spring (0.02–8.02 nmol/L, $n = 231$ versus 0.18–4.20 nmol/L, $n = 27$, respectively). Furthermore, lower DFe and TDFe concentrations in the upper 20 m were observed in inner shelf waters adjacent to sampling line 600, southwest of Anvers Island, during the austral summers of 2015 and 2016 (Sherrell et al., 2018), than documented at our station 20 (Table S1, Fig. S4). These observations suggest a stronger surface source influence and/or lower consumption of DFe due to lower phytoplankton abundance during spring. The implicit underlying assumption is that a change in trace metal inventories is directly related to a change in input or removal fluxes. However, it is important to realize that such changes are not necessarily simultaneous, as the inventory is the result of both current and past fluxes. Inherently, there are uncertainties associated with inferring fluxes based on observed concentrations at fixed points in time that thus should be considered as first order indications. In contrast to the surface ocean, elevated subsurface (70–300 m) DFe and TDFe concentrations (Table S1, Fig. S4) were observed during the summer and spring, suggesting similar processes are controlling subsurface Fe in the inner-shelf waters along sampling line 600 during the two seasons. Alternatively, seasonal changes do not noticeably affect the Fe inventory between seasons at this depth, which could be related, for example, to a longer residence time of Fe in the deeper part of the water column or the position of the sampling location relative to input sources. In our study, the highest SML Fe concentrations generally occurred in Gerlache Strait (DFe = 4.20 nmol/L, TDFe = 73.64 nmol/L) and in the inner shelf stations of sampling lines 700, 600 and 400 (Fig. 2A–B). Based on these values in the SML, higher DFe and possibly particulate Fe (based on higher TDFe) are found over the shelf during spring rather than summer, most likely due to a combination of sedimentary sources, deep winter mixing, winter sea-ice formation and meltwater influence (Section 4.2.). Surface samples collected in summer from the shelf region (Annett et al., 2017; Sherrell et al., 2018) generally have lower DFe and particulate Fe, but cover a wider range of values than spring samples, implying that DFe is removed unevenly by phytoplankton and/or scavenging by settling particles during the growth season. Additionally, DFe as Fe(III) oxyhydroxides could play an important role, despite the relatively high concentrations of unsaturated iron-binding ligands that were observed in samples from the same expedition, ranging from 0.75 to 4.98 nM eq. Fe (Ardiningsih et al., 2021).

Previously, summer surface DFe concentrations of 0.19 ± 0.28 nmol/L ($n = 71$) were observed seaward of the shelf break (Annett et al., 2017). In the current study, spring SML DFe ranged from <0.05–1.40 nmol/L (mean 0.30 ± 0.33 nmol/L, $n = 26$) and TDFe varied from 0.31–7.21 nmol/L (mean 1.77 ± 1.61 nmol/L, $n = 19$). The mean off-shelf Fe concentrations in spring appear higher than in summer. This is not surprising, as prior to the spring, Fe is introduced into the surface ocean via deep winter mixing (Section 4.4.) and winter sea-ice formation (Section 4.2.3.), while the removal of the Fe by phytoplankton is only just starting (Section 4.6.).

4.2. Surface water sources

Surface mixed layer DFe and TDFe increased towards the peninsula, with the lowest DFe and TDFe occurring in off-shelf waters (Section 3.1). This implies that near-surface Fe sources, such as shallow sedimentary input (Sherrell et al., 2018) or surface sources, such as meteoric and sea-ice meltwater (Annett et al., 2017, 2015), are responsible for supplying Fe to the WAP oceanic region, along with additional input from brine rejection and vertical convection during winter sea-ice formation, atmospheric deposition and/or upwelling of intruded CDW at the glacier front by the meltwater pump. It should be noted here that the meltwater pump, as described for the cavities under the ice shelves of the Amundsen Sea, might not act in a similar fashion for the WAP marine terminating glaciers, and other processes, such as wind-driven upwelling and mixing or vertical eddy diffusion near the glaciers or in the coastal region might play a role too.

4.2.1. Atmospheric deposition

Dust particles/aerosols deposited onto the surface waters of the WAP, either directly or indirectly via meltwater input, could have been transported from Patagonia or the Antarctic continent (Bullard et al., 2016). Given the relatively low aerosol deposition rates in our study region (Gao et al., 2020; Gao et al., 2013; Tagliabue et al., 2009),

Table 3
Regressions of DFe concentration vs fraction of meteoric water (%), sea-ice melt (%) and distance (km) in the surface mixed layer.

Transect	DFe versus	Meteoric fraction				Sea-ice melt fraction				Distance			
		r^2	slope	*p*-value	n	r^2	slope	p-value	n	r^2	slope	p-value	n
700*		0,38	0.6 ± 0.3	0,03	12	0,33	−0.4 ± 0.2	0,05	12	0,67	−0.02		12
600		0,48	0.9 ± 0.1	5E-07	41	0,42	−0.7 ± 0.1	4E-06	41	0,58	−0.003		41
400		0,29	1.3 ± 0.5	0,01	20	0,27	−0.9 ± 0.4	0,02	20	0,55	−0.004		20
300		0,38	0.4 ± 0.1	5E-04	28	0,33	−0.3 ± 0.1	0,001	28	0,06	−0.0006		28

* Removing anomalous data at the station 23 resulted in a negative slope for the sea-ice fraction relationship (R2 = 0.33, $p = 0.05$) but a positive slope for the meteoric fraction relationship (R2 = 0.38, $p = 0.03$).

atmospheric deposition is deemed to represent only a minor contribution to the Fe concentrations and distributions along the WAP. However, given that aerosols can accumulate over time on sea ice, glaciers and/or icebergs, the contribution to DFe and TDFe from aerosol-derived Fe could increase when meltwater is released into the ocean during ice melting (Duprat et al., 2019; Gao et al., 2020). The indirect contribution to surface Fe content from atmospheric deposition in the WAP region is difficult to distinguish from meltwater input sources and is not discussed further.

4.2.2. Meteoric meltwater

Meteoric water in the study region is dominantly sourced from meltwater runoff, basal ice melting and free-drifting icebergs (Meredith et al., 2017). Land-derived surface meltwater production in the WAP region is relatively large (>50 mm water equivalent y^{-1}), although most of this meltwater refreezes in the snowpack before reaching coastal waters, which reduces the supply of runoff into coastal waters (van Wessem et al., 2017). The rates of glacial discharge (runoff and basal melting) are largest in the regions around Anvers Island (lines 700 and 600), Adelaide Island (line 300) and southern Palmer Land (not in the sampling grid), and lowest in Marguerite Bay (line 200) and in the northern WAP (van Wessem et al., 2017). The $\delta^{18}O$ results of this study show that the input of meteoric water is highest in the inner shelf waters of sampling lines 600, 400 and 300, with much lower meteoric inputs along sampling line 700 (Fig. 2D). Sampling line 700 was the first transect to become ice-free in the austral spring (Annett et al., 2017) and strong currents (Savidge and Amft, 2009) could have diluted the meteoric fraction. In contrast, lines 600, 400 and 300 still had some ice cover during the sampling period (Arrigo et al., 2017) preventing wind stress, and hindering wind-driven currents and mixing. Furthermore, the correlation of DFe with distance landward implies the SML Fe in the study region cannot just be attributed to meteoric melt, as additional shelf processes could also contribute sources of Fe. Notably, the meltwater pump or other coastal mixing processes that bring Fe from deeper waters with associated sediment input would also lead to coinciding increases in both Fe and the meltwater fraction, where only part of the Fe has a meltwater origin (van Leeuwe et al., 2020; St-Laurent et al., 2017; St-Laurent et al., 2019), as would nearby shallow sedimentary Fe sources (Sherrell et al., 2018).

Nevertheless, glaciers, through melting into coastal waters (Annett et al., 2017, 2015), or icebergs melting into the shelf and/or off-shelf waters (Lin et al., 2011), can provide sources of Fe to the Southern Ocean. Notably, basal ice and icebergs can have very high Fe contents due to lithogenic particulate material in the ice, and respective DFe and TDFe as high as 607 nmol/L and 1900 nmol/L in icebergs (Hopwood et al., 2019; Lin et al., 2011), and median values of 0.98 and 108.87 μmol/L in glacial meltwater runoff from the Antarctic Peninsula (Hodson et al., 2017), have been reported. In this study, the DFe of the meteoric meltwater endmember was estimated as 78 ± 38 nmol/L using the regression of DFe versus the meteoric fraction in seawater (Tables 3 and 4), and is an underestimate because conservative behavior of Fe is assumed. This value agrees well with a previous estimate of 66 ± 108 nmol/L for this region (Annett et al., 2017), but is lower than the DFe measured directly in local and Antarctic Peninsula glacial meltwater of 348 ± 14 nmol/L (Annett et al., 2017) and 980 nmol/L, respectively (Hodson et al., 2017). This discrepancy is most likely due to the removal of DFe via scavenging, both in the strong salinity gradient upon delivery to the water column as well as during advection to the sampling location, as such high concentrations of Fe cannot be maintained in dissolved form in oxygenated seawater. Overall, meteoric water appears to be an important source of Fe to the study region, but based on currently available data, the exact contribution cannot be quantified with certainty.

Table 4
Regressions of DFe concentration vs fraction of meteoric water (%) in the surface mixed layer and an estimation of the pure meteoric endmember DFe concentration.

Transect	Slope (nmol/L/%met)	y-intercept (nmol/L/%met)	r^2	p-value	DFe in endmember (nmol/L) ± CI (95%)
300	0.4 ± 0.1	−0.8 ± 0.3	0,38	4E-04	41 ± 21
400	1.3 ± 0.5	−4.0 ± 1.7	0,29	0,01	127 ± 97
600	0.9 ± 0.1	−1.5 ± 0.4	0,48	5E-07	84 ± 28
700	0.6 ± 0.2	−1.0 ± 0.7	0,38	0,03	59 ± 53
		Mean estimate (±1SD)			**78 ± 37**

4.2.3. Sea-ice

Another source of Fe into surface water is sea-ice melt and winter sea-ice formation. Dissolved Fe in sea ice cores range from 0.23–81.0 nmol/L e.g. (van der Merwe et al., 2011), generally higher than in underlying water (e.g. Lannuzel et al., 2014; Schallenberg et al., 2016).

In this study, a negative correlation between DFe and sea ice melt fraction was generally found in the SML (Table 3), with higher DFe observed in regions with a sea-ice formation signature (negative sea-ice meltwater fraction) (Fig. 2A–C). This indicates that a winter sea-ice formation signal is still present during the spring sampling period of this study, as has also been observed in this and other regions during summer (Meredith et al., 2008; Meredith et al., 2017; 2013; Randall-Goodwin et al., 2015). The elevated DFe and TDFe in regions with a sea-ice formation signature could be due to Fe release into seawater via brine rejection (Schallenberg et al., 2016) or through the resulting vertical convection (Williams et al., 2011) that brings up Fe from underlying waters, especially over shallow parts of the shelf where near-bottom DFe and TDFe levels are high (Fig. 3). The strongest sea ice formation signature was generally found at the inner shelf stations (Fig. 2C) where ice cover is the last to melt, preventing wind-induced mixing and probably preserving the sea-ice formation signature longer. For the remaining shelf waters, the winter sea-ice formation signature is likely diluted due to wind driven mixing and meltwater input from both sea-ice and meteoric meltwater. In contrast to spring, a positive correlation between the sea-ice meltwater fraction and both DFe and particulate Fe was observed in summer (Annett et al., 2017). It appears spring is more dynamic than summer, as the effects of both ice formation and ice melt are generally still detectable, and sea-ice formation, meteoric meltwater, the meltwater pump and/or other coastal mixing processes, are likely to be important sources of Fe to the euphotic zone.

4.2.4. Antarctic Peninsula coastal current (APCC)

A noteworthy feature of the shelf is the formation of the APCC current in the surface water layer during the ice melt period resulting from meltwater runoff (Moffat et al., 2008; Moffat and Meredith, 2018). During our sampling period, the exact location of the APCC could not be defined. However, the APCC is known to traverse the inner shelf waters of sampling lines 700, 600, 400 and 300 (Fig. 1A, yellow line), and the APCC can be identified by a deepening of the mixed layer (e.g. Moffat and Owens, 2008). A deepening to ~110 m, indicative of the APCC, was indeed observed for the inner shelf stations (stations 70, 71, 72, 73) of sampling lines 400 and 300 (Fig. 3E–H, S2C–D). Interestingly, SML DFe and TDFe content was low in the inner shelf of sampling line 300, but was elevated at sampling line 400, indicating that DFe input at line 400 does not extend to line 300, or it was transported in a different branch of the current that was not sampled. It seems likely that the APCC current is important for transporting DFe from Anvers Island along Briscoe and Adelaide Islands into Marguerite Bay where it joins the seaward flow out of Marguerite Bay, potentially transporting DFe from the northeast of the shelf towards the southwest and out towards the off-shelf area (Moffat and Meredith, 2018; Savidge and Amft, 2009). Unfortunately, this region was not investigated during our study, but a high surface Fe content in Marguerite Bay during summer could be associated with meteoric meltwater input and/or shallow sedimentary sources

transported within the APCC, in combination with basal melt from the George VI ice shelf. The APCC current could therefore be crucial in supporting productivity in the off-shelf waters seaward of Marguerite Bay, especially during the summer when the current becomes stronger (Moffat and Meredith, 2018; Savidge and Amft, 2009; Marrari et al., 2008; Annett et al., 2017) and should be investigated in future studies. The APCC also flows in the opposite direction to the northeast between the Antarctic Peninsula and Anvers and Brabant Islands through Gerlache Strait towards the South Shetland Islands (Fig. 1A) (Moffat and Meredith, 2018; Savidge and Amft, 2009). In this strait, the highest SML DFe and TDFe of the whole dataset were observed. Below the surface, DFe and TDFe decreased with depth in the upper 100 m, then increased with depth below 100 m (Fig. S8A). The elevated deeper concentrations are most likely related to non-reductive sedimentary input (Section 4.3), whereas the elevated surface concentrations are probably related to the formation of the APCC current and the associated freshwater discharge from the surrounding islands and Peninsula. However, the estimated meteoric meltwater fraction was not high relative to other inner-shelf estimates, implying a range in meteoric meltwater endmembers or a dominant contribution from shallow sedimentary sources (Sherrell et al., 2018). Overall, despite a lack of direct evidence for the role of the APCC in supplying Fe to surface waters in Gerlache Strait, the findings of this study suggest that the APCC could be important for the transport of Fe in this region. However, this interpretation might be biased by the location of the single station in the Gerlache Strait where the proximity to the coastline could also play an important role in surface Fe supply.

4.3. Sedimentary sources

Sedimentary sources play a major role in providing Fe to the shelf waters of the WAP, as is apparent from the elevated DFe and TDFe observed in the bottom shelf waters of the study area (Fig. 3). Sedimentary Fe can be brought up in the water column through diffusion of DFe, the resuspension of sedimentary particles via overflow-driven mixing caused by the bathymetric features of the seafloor of the WAP shelf (Venables et al., 2017), deep shelf break mixing and buoyancy-driven circulation (de Jong, 2012; St-Laurent et al., 2017; Venables et al., 2017) or directly from shallow sediments (Sherrell et al., 2018). According to a modeled Fe budget, approximately 27% of the total Fe input into the shelf region of Antarctica is derived from a sedimentary flux from the extensive continental shelf (Tagliabue et al., 2009). Sedimentary sources of Fe to the shelf region of the study area are especially important for sampling lines 700, 300 and 200 (Fig. 3A–B, G–J) given the relatively high bottom water concentrations at these locations, but elevated near-bottom concentrations are observed along all sampling lines (Fig. 3C–F). High productivity in surface waters can lead to buildup of organic matter in the underlying sediments, resulting in low oxygen conditions and reductive dissolution of Fe (Annett et al., 2017). Due to the faster oxidation and precipitation of Fe relative to Mn in overlying oxygenated seawater, reductive dissolution should lead to a higher effective release of Mn than Fe, and a higher DMn:DFe ratio (Hatta et al., 2013) unless Fe is stabilized by high concentrations of organic ligands present in the water column (Ardiningsih et al., 2021). A higher average inshore DMn:DFe ratio (5.9 ± 3.6 mol:mol) was observed in the more productive near-surface waters of the northern lines than the lower productivity southern lines (1.2 ± 1.2 mol:mol) during the 2011 and 2012 Pal-LTER summer sampling campaigns, and was attributed to reductive sedimentary processes (Annett et al., 2017). During the spring period of the current study, the SML DMn:DFe ratio (1.82 ± 0.61 mol:mol; Table 5) on the shelf was close to the value (1.2 ± 1.2 mol:mol) observed for the lower productivity southern lines of the 2011 summer campaign (Annett et al., 2017). This could imply that high productivity-driven reductive sedimentary processes were not yet operating in spring, or alternatively, that the summer drawdown of DFe drives Mn:Fe ratios to higher values without a seasonal change in DMn.

A signature of reductive sedimentary input on the shelf is more likely to be observed below the permanent pycnocline (160 m, Couto et al., 2017). However, the relatively low DMn:DFe ratio (0.62 ± 0.31 mol:mol; Table 5) on the shelf below 160 m depth demonstrates a higher concentration of DFe than DMn. The presence of such low DMn:DFe ratios contradicts the influence of reductive dissolution of Mn and Fe from sediments on the shelf during the sampling period. Instead of reductive dissolution, a possible mechanism that could lead to the non-reductive sedimentary input of Fe (Homoky et al., 2013) and Mn below the pycnocline is the resuspension of sedimentary particles, followed by desorption from (likely authigenic) phases.

High energy physical processes such as wind-induced wave action (Gargett et al., 2004) and tidal currents (De Jong et al., 2015) can lead to the resuspension of sedimentary particles, forming nepheloid layers in intermediate and bottom waters (de Jong, 2012). Additionally, in the current study region, CDW intrusion through troughs via eddy events (Couto et al., 2017; Martinson and McKee, 2012; Martinson et al., 2008; Moffat and Meredith, 2018; Moffat et al., 2009) or overflow-driven mixing (Venables et al., 2017) could also cause resuspension. Indeed, a nepheloid layer was observed based on relatively low beam transmission close to the seafloor that coincided with increased DFe and TDFe (Fig. S8–9). The shallow ridge near the coast along sampling line 300 could induce transport of DFe from deeper depths into the SML, increasing Fe content, but this was not evident from CTD data as the overlying water column was well stratified (Fig. S2). Moreover, SML DFe and TDFe concentrations overlying the ridge were relatively low, also implying an absence of Fe supply via local upwelling. In contrast, along lines 400, 600 and 700, elevated SML and subsurface (shallower than 200 m) DFe and TDFe were observed over the shelf, but again the strong stratification implies no direct local upwelling (Fig. S2, S7). Some outcropping of near-surface isopycnals can be observed at the shelf break, but strong stratification in subsurface waters at these locations implies that there was no recent deep shelf break mixing (Figs. S2, S6). Most likely, upwelling of deep Fe via the meltwater pump or other mixing processes close to the coast play a role, but given that SML and subsurface DFe and TDFe are generally higher than deep concentrations, an additional source of Fe is required. The latter is most likely meltwater or advection from nearby shallow sedimentary sources.

Table 5
Mn:Fe ratio in the study region. Labile particulate (lp) = total dissolvable – dissolved concentration.

			Upper surface layer (<10 m)	SML	Permanent Pycnocline	Below Pemanent Pycnocline
Shelf	dMn:dFe	mol:mol	1.82 ± 0.61	1.94 ± 0.67	1.68 ± 0.76	0.62 ± 0.31
	lpMn:lpFe	mol:mol	0.028 ± 0.015	0.034 ± 0.027	0.034 ± 0.023	0.042 ± 0.019
Shelf slope	dMn:dFe	mol:mol	2.33 ± 1.58	2.10 ± 1.55	2.01 ± 1.31	0.70 ± 0.33
	lpMn:lpFe	mol:mol	0.060 ± 0.030	0.053 ± 0.031	0.060 ± 0.033	0.046 ± 0.020
Off-shelf	dMn:dFe	mol:mol	0.93 ± 0.53	1.12 ± 0.63	1.24 ± 0.69	0.80 ± 0.26
	lpMn:lpFe	mol:mol	0.16 ± 0.18	0.27 ± 0.49	0.22 ± 0.44	0.13 ± 0.23
Gerlache Strait	dMn:dFe	mol:mol	0.87 ± 0.01	0.86 ± 0.02	0.84 ± 0.06	0.36 ± 0.05
	lpMn:lpFe	mol:mol	0.017 ± 0.001	0.017 ± 0.001	0.017 ± 0.001	0.016 ± 0.001
Inner Shelf	dMn:dFe	mol:mol	1.54 ± 0.32	1.63 ± 0.57	1.32 ± 0.61	0.66 ± 0.45
	lpMn:lpFe	mol:mol	0.023 ± 0.010	0.026 ± 0.013	0.027 ± 0.008	0.035 ± 0.017

Based on the current observations, non-reductive sedimentary input of DFe is likely prominent during the spring, and is possibly mediated by ligands (Ardiningsih et al., 2021) or supplied by small colloids (Homoky et al., 2013). This is not surprising given that low phytoplankton growth during spring, inhibited by ice cover, likely results in lower organic matter build-up in shelf sediments and deeper oxygen penetration, whereas higher productivity in summer would lead to higher organic matter and lower oxygen in shelf sediments, facilitating reductive Fe release (Hatta et al., 2013). Interestingly, the breakdown of organic matter can result in both the production of ligands (Ardiningsih et al., 2021) as well as the consumption of oxygen, where different ligands are likely involved in non-reductive solubilization of Fe(III) compared to maintaining Fe(II) in solution from reductive dissolution, which could be the subject of future studies. We suggest that during spring, DFe is introduced from sediments, as the intrusion of CDW in combination with bathymetric features leads to resuspension and desorption of bound Fe from sediment particles, or mixing of porewater into overlying water, increasing bottom water DFe. The influence of sedimentary sources is indeed seen in the increasing DFe in UCDW during its transport landward across the shelf where the initial concentration of 0.37 ± 0.17 nmol/L (mean with 1 SD in off-shelf UCDW) increases to 0.91 ± 0.36 nmol/L (mean with 1 SD in on shelf CDW) in intruded CDW over the shelf that will contribute to SML Fe concentrations after coastal upwelling or mixing.

4.4. Horizontal and vertical Fe supplies

It has been hypothesized that during winter, DFe-rich deep water is entrained into the surface ocean, increasing productivity in the off-shelf waters of the Southern Ocean in the next growth season (Tagliabue et al., 2014). It has also been proposed that winter mixing could supply ten times more Fe than diapycnal diffusion to the surface ocean each year (Tagliabue et al., 2014). During the early austral spring, DFe was low at the off-shelf stations where elevated DFe was observed below the permanent pycnocline, implying that winter mixing was not deep enough to tap into elevated deep Fe sources (Figs. S2 and S5). Thus, significant entrainment of 'deep DFe' is not likely and any DFe present in the SML after winter is removed rapidly, potentially by sea ice algae or by the growing phytoplankton community, as suggested by elevated chlorophyll *a*.

Even though DFe was low in the SML during the spring sampling season, primary producers were active at the off-shelf stations and phytoplankton were not yet suffering from Fe stress (Arrigo et al., 2017; Joy-Warren et al., 2019). Net primary productivity was especially high at the stations located between the SACCF and SBACC fronts (Joy-Warren et al., 2019), which was attributed to the upwelling of DFe rich waters at this location (Arrigo et al., 2017). However, these elevated productivity levels could potentially also be from a lateral shelf flux of Fe, similar to observations in the offshore regions of Drake Passage (Dulaiova et al., 2009) and the upper mixed layer of the Atlantic Sector of the Southern Ocean (de Jong, 2012).

As discussed previously in Sections 4.2 and 4.3, the shelf waters of the study region had a high inventory of DFe that could be transported from the shelf to the off-shelf region. The estimated supplies (horizontal and vertical) have a wide range due to the range of adopted K_h and K_z values (see Section 2.4) as well as the variable influence of the different Fe sources along the sampling transects. Therefore, we use median supply values per area (inner shelf, mid-shelf, shelf break, continental slope and frontal regions) of the combined transects instead of average values to decrease the influence of the extreme values on the supply estimate (Table 6). As expected, the magnitude of the supply decreased with increasing distance from the peninsula and increasing water column depth, with the highest supplies derived for the inner shelf stations (Table 6). The horizontal supply (2.7–40.1 μmol m^{-2} d^{-1}; median of all transects for a low and high K_h, respectively) into the SML is higher than the vertical supply (0.2–0.3 μmol m^{-2} d^{-1} median of all transects for low and high K_z, respectively) for the inner shelf, which is most likely due to the proximity of sources. Similarly, a stronger influence of the horizontal supply was observed below the SML in inner shelf waters (Table 6). However, with increasing distance from the shore, the vertical supply of Fe becomes higher than the horizontal supply (Table 6). Besides using power functions (see Section 2.5), the horizontal and vertical supplies were also estimated using an exponential function after Gerringa et al. (2012). This also gave larger vertical than horizontal supplies beyond the shelf break and vice versa over the shelf. The Fe inventories and estimated supplies in the SML are compared to the calculated Fe demand (Sections 4.5 and 4.6) to see if the inventory or the combined horizontal and vertical supply is sufficient to support productivity during spring, summer and the whole growing season (spring + summer) over the shelf and beyond the shelf break (off-shelf).

Despite the overall strong attenuation of Fe horizontal supplies towards the off-shelf region, it is evident from the DFe distribution (Fig. 3), that elevated Fe persists further off-shore in the subsurface. This implies that some of the subsurface horizontal Fe supply contributes to the vertical supplies into the SML close to the shelf by generating stronger vertical Fe gradients but this effect becomes negligible in off-shelf waters where elevated Fe was only found below the permanent pycnocline as discussed previously.

The horizontal supply in SML decreased off-shelf, suggesting that continentally derived Fe is largely confined to the shelf and shelf break

Table 6
Estimated DFe supplies in and below the surface mixed layer. SML – surface mixed layer; BSML – below surface mixed layer.

		Vertical Supply[a]		Horizontal Supply[a]	
	Water column	Low	High	Low	High
		μmol/m^2/d	μmol/m^2/d	μmol/m^2/d	μmol/m^2/d
Inner Shelf	SML	0.2 [0.07–0.3] (*n* = 5)	0.3 [0.1–0.6] (n = 5)	2.7 [2.2–4.4] (*n* = 3)	40.1 [32.2–65.5] (n = 3)
	BSML	0.1 [0.07–0.3] (n = 5)	0.2 [0.1–0.7] (n = 5)	4.5 [2.1–6.1] (n = 3)	71.8 [33.6–97.1] (n = 3)
Mid-shelf	SML	0.06 [0.06–0.07] (n = 5)	0.1 [0.1–0.1] (n = 5)	0.05 [0.04–0.2] (n = 4)	0.7 [0.5–2.2] (n = 4)
	BSML	0.07 [0.05–0.2] (n = 5)	0.1 [0.07–0.3] (n = 5)	0.06 [0.03–0.3] (n = 4)	1.0 [0.5–4.0] (n = 4)
Shelf Break	SML	0.05 [0.03–0.06] (n = 4)	0.08 [0.05–0.1] (n = 4)	0.01 [0.007–0.02] (n = 4)	0.2 [0.1–0.3] (n = 4)
	BSML	0.07 [0.04–0.1] (n = 4)	0.1 [0.06–0.2] (n = 4)	0.02 [0.007–0.02] (n = 4)	0.3 [0.1–0.3] (n = 4)
Continental Slope	SML	0.04 [0.02–0.07] (n = 4)	0.07 [0.04–0.2] (n = 4)	0.006 [0.003–0.01] (n = 4)	0.08 [0.04–0.2] (n = 4)
	BSML	0.03 [0.02–0.06] (*n* = 4)	0.06 [0.03–0.08] (*n* = 4)	0.007 [0.004–0.01] (*n* = 4)	0.1 [0.07–0.2] (*n* = 4)
SBACC[b]-SACCF[c]	SML	0.01 [0.008–0.02] (n = 7)	0.03 [0.02–0.05] (n = 7)	0.001 [0.0004–0.005] (n = 7)	0.02 [0.006–0.07] (n = 7)
	BSML	0.02 [0.019–0.03] (n = 7)	0.04 [0.02–0.05] (n = 7)	0.002 [0.0005–0.004] (n = 7)	0.03 [0.008–0.07] (n = 7)
NW of SACCF[c]	SML	0.009 [0.008–0.01] (n = 7)	0.02 [0.01–0.03] (n = 7)	0.0004 [0.0003–0.001] (n = 7)	0.005 [0.005–0.02] (n = 7)
	BSML	0.01 [0.01–0.02] (n = 7)	0.02 [0.02–0.04] (n = 7)	0.0004 [0.0003–0.001] (n = 7)	0.007 [0.005–0.02] (n = 7)

[a] Median values with minimum and maximum values indicated between box brackets and number values (n) calculated for each region in the sampling area.
[b] SBACC – Southern Boundary of Antarctic Circumpolar Current.
[c] SACCF – Southern Antarctic Circumpolar Current Front.

regions above the permanent pycnocline. This decrease can be observed in the average DFe and TDFe in and below the SML where Fe decreases by 80–90% from shelf to off-shelf waters (Table 2). When productivity increases on the shelf during summer, a further decrease of the lateral Fe flux is expected as a consequence of biological assimilation into, and scavenging onto biogenic particles. Therefore, we deem it likely that continentally derived Fe is largely confined to the WAP shelf region, not only as a result of the local hydrography as suggested previously (Sieber et al., 2021), but also as a result of scavenging and biological uptake.

4.5. Phytoplankton uptake

We observed low DFe in off-shelf SML (<0.1 nmol/L), below the assumed threshold for growth limitation of oceanic phytoplankton (Sedwick et al., 2011), but conversely, relatively high chlorophyll *a* provides no indication of Fe limitation (Arrigo et al., 2017). The parameter Fe* represents the product of the uptake ratio Fe:N or Fe:P and the nitrate or phosphate concentration subtracted from the DFe (Holmes et al., 2019; Parekh et al., 2005). Depending on the uptake rate of Fe by phytoplankton based on taxonomic and physiological controls on intracellular Fe:C:N:P ratios, one can determine if primary productivity is more likely to be limited by either DFe (negative Fe*) or the macronutrients nitrate or phosphate (positive Fe*) (Table S2). This approach is often done to assess the potential for Fe limitation in subsurface waters prior to upwelling, but is used here for the SML to assess the likelihood that this layer will evolve to Fe limitation over time. Either way, this approach has several underlying assumptions: (1) no preferential remineralization of Fe (or nitrate or phosphate, i.e. nutrients remineralize in unison), (2) the inventories observed are representative of the rest of the season with either no additional input, or any additional input is matched by abiotic loss factors, and (3) all DFe is bioavailable and not lost via scavenging (Boyd et al., 2017; Rafter et al., 2017; Richon et al., 2020). When Fe* is derived using an intermediate Fe:C ratio of 10 μmol:mol (Twining et al., 2004), nitrate or phosphate is predicted to become a limiting nutrient at the inner shelf stations where there is a high inventory of Fe (Table S2) and DFe is the limiting nutrient everywhere else, as was suggested before (Annett et al., 2017; Sherman et al., 2020). When a low Fe:C uptake ratio of 1.7 μmol:mol (Twining and Baines, 2013) is adopted, then stations located on the shelf as well as the continental slope are considered to become limited by nitrate or phosphate. Relatively low, but not depleted concentrations of nitrate (2.20 μmol/L) and phosphate (0.10 μmol/L) have been observed during late summer in a coastal bay (Ryder Bay; van Leeuwe et al., 2020), suggesting that major nutrients are not usually limiting in regions near to the major sources of Fe. Given the proximity to Fe sources, other factors such as light limitation most likely prevent full macronutrient depletion (e.g. Twelves et al., 2021). Alternatively, when an extremely high Fe:C uptake ratio of 40 μmol:mol (Twelves et al., 2021) is used, then DFe is predicted to be the limiting nutrient at all stations. We chose to use different uptake ratios for these calculations, since during early spring, a relatively high uptake ratio is expected, and as the season progresses, the availability of Fe decreases, likely resulting in a decreasing uptake ratio. Such a change in Fe availability could lead to changes in community composition. Indeed, a shift from a *Phaeocystis antarctica*-dominated community to a diatom-dominated community was observed in spring (Arrigo et al., 2017; Joy-Warren et al., 2019), linked to changes in light intensity and possibly a depletion of Fe. The results of this study show that the DFe inventory in off-shelf waters is low from the beginning of the growth season (early austral spring), indicating that most DFe had already been consumed by the phytoplankton community, potentially resulting in Fe limitation in the beginning of the summer season. On the contrary, inner shelf waters have a sufficiently high DFe inventory to potentially deplete the macronutrient inventory during the growth season, whereas mid-shelf phytoplankton communities could only deplete macronutrients by adapting to a lower Fe uptake ratio. However, these estimates are based on a snapshot in time, and most likely there was a continuous supply of nutrients throughout the season, such as via CDW upwelling or sedimentary supply, as well as remineralization of the nutrients from accumulated biogenic particulate matter.

4.6. Fe demand

Here, we compare Fe supplies with Fe demand from primary productivity, converting satellite-based net primary productivity (NPP) estimates from Joy-Warren et al. (2019), in mol C/m^2/d, to Fe demand, in μmol Fe/m^2/d, using different Fe uptake ratios (see Section 4.5). The underlying rationale is that the combination of calculated vertical and horizontal inputs as the total supply should be sufficient to support productivity during the growth season.

It has been suggested that light is the growth-limiting factor during the sampling period of our study (Arrigo et al., 2017; Joy-Warren et al., 2019; Oliver et al., 2019), and it is likely that Fe limitation develops later in the season, especially off-shelf. Therefore, here we assess if the horizontal DFe supply into the SML from the shore to the off-shelf, and/or the vertical supply from underlying waters into the SML is sufficient, either separately or combined, to support the estimated NPP throughout the season (Table 7), noting that these are first order supply estimates with large uncertainties (see Section 2.4). As detailed in Section 4.4, we used the median value of the estimated supplies per area, calculated using the upper and lower limits for diffusivity and advection coefficients.

Our estimated supply resulting from the horizontal flux to the entire sampling area (0.005–0.07 μmol m^{-2} d^{-1}, assumed to be constant during the season) is not enough to support average NPP for all growth over the entire season in the region under moderate (Fe:C ratio of 10 μmol:mol) or high (Fe:C ratio of 40 μmol:mol) uptake ratios. Even with a low uptake ratio (Fe:C ratio of 1.7 μmol:mol), average NPP can only be supported with high diffusivity coefficients (Table 7). The horizontal supply to off-shelf waters (0.001–0.02 μmol m^{-2} d^{-1}), is only sufficient to support average NPP if a high diffusivity coefficient is assumed and when using a low uptake ratio (Fe demand of 0.015 ± 0.006 μmol m^{-2} d^{-1}). In contrast, horizontal supply over the shelf (0.05–0.7 μmol m^{-2} d^{-1}) should be sufficient to support NPP under any uptake ratio (Table 7). These results again suggest that horizontal supply within the SML might not be an important source of the limiting micronutrient Fe for the off-shelf region.

The calculated supply via the vertical flux (0.03–0.05 μmol m^{-2} d^{-1}, assumed to be constant during the season) is only sufficient to support the average estimated NPP under a low uptake ratio for all regions and seasons (Table 7). The estimated supply of the total flux (sum of horizontal and vertical supply) is only high enough to support average NPP under low uptake ratios in the off-shelf region and under low, moderate, or high uptake ratios in the shelf region. These supply estimates might only be representative of the early spring, as even lower SML Fe concentrations occur during summer, with relatively invariant deep water concentrations, implying a stronger vertical gradient in summer that will enhance vertical supply. Nevertheless, these estimations imply that the phytoplankton community has a relatively low average uptake ratio that is likely between 1.7 and 10 μmol:mol Fe:C in the off-shelf region and in the range of 10 to 40 μmol:mol Fe:C for the shelf region during the sampling period of this study.

The large range and variation in the supply of Fe between different locations (Table 5) supports the hypothesis of patchy Fe limitation in WAP shelf waters (Garibotti et al., 2003; Prézelin et al., 2004; Smith et al., 2008) as well as heterogeneous Fe inputs (Annett et al., 2017). Additionally, the results of our study suggest that the horizontal flux has a greater influence on the supply of Fe in the shelf region than in the off-shelf region (Section 4.4.), which is not surprising given the proximity of Fe sources, such as glaciers and shallow sediments. In contrast, the influence of the vertical flux is dominant in the off-shelf region (Section 4.4).

Table 7
Net primary productivity (NPP) and estimated DFe demand.[a, b, c]

	NPP	Fe Demand			Vertical[a] Supply	Horizontal[a] Supply	Total Supply[b]	
		Low	Medium	High			Low	High
	mol C/m^2/d	μmol/m^2/d	μmol/m^2/d	μmol/m^2/d	μmol/m^2/d	μmol/m^2/d	μmol/m^2/d	μmol/m^2/d
Sampling area during entire growth season	0.011 ± 0.004	0.018 ± 0.007	0.11 ± 0.04	0.42 ± 0.17	0.03–0.05	0.005–0.07	0.03 [0.008–4.6] (n = 29)	0.1 [0.02–65.8] (n = 29)
Off-shelf region during entire growth season	0.009 ± 0.003	0.015 ± 0.006	0.09 ± 0.03	0.36 ± 0.14	0.01–0.02	0.001–0.02	0.01 [0.008–0.07] (n = 18)	0.04 [0.02–0.3] (n = 18)
Shelf region during entire growth season	0.018 ± 0.010	0.03 ± 0.02	0.18 ± 0.10	0.73 ± 0.40	0.06–0.1	0.05–0.7	0.1 [0.04–4.6] (*n* = 11)	0.8 [0.2–65.8] (n = 11)
Sampling area during spring season[c]	0.010 ± 0.003	0.017 ± 0.005	0.10 ± 0.03	0.40 ± 0.12	0.03–0.05	0.005–0.07	0.03 [0.008–4.6] (*n* = 29)	0.1 [0.02–65.8] (n = 29)
Sampling area during summer season	0.013 ± 0.004	0.022 ± 0.008	0.13 ± 0.04	0.53 ± 0.18	0.03–0.05	0.005–0.07	0.03 [0.008–4.6] (n = 29)	0.1 [0.02–65.8] (n = 29)

[a] Median values of vertical and horizontal supplies based on a high and low K_z and K_h.
[b] Median values with minimum and maximum values indicated between box brackets and number of values calculated for each region in the sampling area.
[c] Same vertical and horizontal supplies for spring and summer seasons.

5. Conclusions

In the present study, samples were collected across a range of water depths, in order to assess the depth distributions as well as the surface concentrations of DFe and TDFe during the austral spring in one of the regions of Antarctica that is being strongly impacted by changing climate. In the WAP oceanic region, elevated meteoric meltwater fractions and the presence of a sea-ice formation signal coincided with high DFe and TDFe in the SML. Deeper in the water column, the benthic release of DFe (e.g. resuspended sedimentary particles and/or pore-waters) was inferred, suggesting an important role for sediment resuspension as a result of CDW intrusion and overflow mixing facilitated by the bathymetric features of the shelf. The concentrations of DFe and TDFe in spring appear to be mainly controlled by the influence of sea-ice formation during the preceding winter, and the supply of Fe from meteoric meltwater and from below via coastal upwelling or mixing, or supply from nearby shallow sediments. To improve understanding of the Fe distribution and the potential for horizontal and vertical transport, higher resolution sampling is needed to constrain the influence of small-scale features, such as intruding eddies, and heterogeneous sources. Additionally, characterization of the sedimentary pore-water biogeochemistry during spring and summer could reveal if indeed Fe is mainly released via non-reductive dissolution or if there is a seasonal progression towards reductive dissolution, and how this might change in this rapidly changing environment.

Antarctic Peninsula glaciers have undergone significant retreat due to an increase in surface air temperature and ocean forcing, primarily via the intrusion of relatively warm CDW waters onto the shelf (Cook et al., 2016). Antarctic ice sheet retreat has been suggested to result in an increase in lateral Fe supply from meltwater (Death et al., 2014; Wadham et al., 2013) but input from shallow sediments combined with coastal upwelling or mixing has been suggested as another, and potentially even more important source of Fe into the surface water (e.g. St-Laurent et al., 2019; Twelves et al., 2021). Estimated DFe supplies for the current study region suggest that the horizontal supply into the SML is higher than the vertical supply for shelf stations. However, the vertical supply becomes more prominent seaward where it becomes the largest supply, notably between SBACC and SACCF as suggested before (Arrigo et al., 2017). The majority of DFe and TDFe introduced into shelf waters is removed in the shelf region prior to reaching off-shelf waters in either the SML or the subsurface. Consequently, the calculated horizontal supply is currently estimated to be insufficient to support the observed net primary productivity in the off-shelf region. Thus, a future increase in Fe input might not have profound consequences for Fe availability in off-shelf waters. Furthermore, the currently estimated total supply into the off-shelf SML is barely enough to support observed net primary productivity throughout the growth season. This is opposite to the shelf region where the total flux supplies enough Fe to maintain observed NPP, even when assuming a high Fe:C uptake rate. If the trend of a decrease in sea-ice cover continues, this could result in a lower supply of Fe from below in the off-shelf region. Such a decrease in the vertical flux would be due to a smaller region of winter entrainment that is driven by brine rejection during sea-ice formation that deepens the mixed layer depth (Tagliabue et al., 2014). Additionally, increasing melt rates and water temperatures might result in stronger stratification in the surface layer and weaker vertical diffusivity between the surface water layer and the water beneath the pycnocline (Sarmiento et al., 2004) but the consequences of stronger stratification on nutrient supply from below are subject to ongoing discussion (van Haren et al., 2021). Overall, predictions about the future of iron cycling and its effect on primary productivity in WAP waters and the Southern Ocean remain uncertain, and it is abundantly clear that many intricacies of this unique and interconnected system remain unresolved.

Declaration of Competing Interest

None.

Acknowledgments

We thank the captain and the crew of the RVIB *Nathaniel B. Palmer* for their assistance during the cruise. We also thank the Phantastic II research team who were essential in procuring samples and Dr. Loes Gerringa for her insightful comments that greatly improved this manuscript. This work was supported by a grant from the National Science Foundation Office of Polar Programs to K.R.A. (ANT-1063592), the University of Otago Doctoral Scholarship, the Centre for Trace Element Analysis and the Ocean Systems Department of NIOZ. Samples were collected as part of the GEOTRACES Process Study (GPpr08) and data can be found in the GEOTRACES database as part of the 2021 Intermediate Data Product (doi:10.5285/cf2d9ba9-d51d-3b7c-eo53-8486abc0f5fd).

Appendix A. Supplementary data

Supplementary data to this article can be found online at https://doi.org/10.1016/j.marchem.2021.104066.

References

Annett, Amber L., Skiba, Marta, Henley, Sian F., Venables, Hugh J., Meredith, Michael P., Statham, Peter J., Ganeshram, Raja S., 2015. Comparative roles of upwelling and glacial iron sources in Ryder Bay, coastal western Antarctic Peninsula. Mar. Chem. 176, 21–33. https://doi.org/10.1016/j.marchem.2015.06.017.

Annett, Amber L., Fitzimmons, Jessica N., Séguret, Marie J.M., Lagerström, Maria, Meredith, Michael P., Schofield, Oscar, Sherrell, Robert M., 2017. Controls on dissolved and particulate iron distributions in surface waters of the Western Antarctic Peninsula shelf. Mar. Chem. 196, 81–97. https://doi.org/10.1016/j.marchem.2017.06.004.

Arrigo, Kevin R., van Dijken, Gert L., Bushinsky, Seth, 2008. Primary production in the Southern Ocean, 1997–2006. Journal of Geophysical Research Oceans 113. https://doi.org/10.1029/2007JC004551.

Ardiningsih, Indah, Seyitmuhammedov, Kyyas, Sander, Sylvia G., Stirling, ClaudineH., Reichart, Gert-Jan, Arrigo, Kevin R., Gerringa, Loes J.A., Middag, Rob, 2021. Fe-binding organic ligands in coastal and frontal regions of the western Antarctic Peninsula. Biogeosciences 18, 4587–4601. https://doi.org/10.5194/bg-18-4587-2021.

Arrigo, Kevin R., van Dijken, Gert L., Alderkamp, Anne-Carlijn, Erickson, Zachary K., Lewis, Kate M., Lowry, Kate E., Joy-Warren, Hannah L., Middag, Rob, Nash-Arrigo, Janice E., Selz, Virginia, van de Pol, Willem, 2017. Early spring phytoplankton dynamics in the Western Antarctic peninsula. J Geophys Res-Oceans 122, 9350–9369. https://doi.org/10.1002/2017JC013281.

Barrand, N.E., Vaughan, D.G., Steiner, N., Tedesco, M., Kuipers Munneke, P., van den Broeke, M.R., Hosking, J.S., 2013. Trends in Antarctic peninsula surface melting conditions from observations and regional climate modeling. J. Geophys. Res. Earth Surf. 118, 315–330. https://doi.org/10.1029/2012JF002559.

Biller, Dondra V., Bruland, Kenneth W., 2012. Analysis of Mn, Fe, Co, Ni, Cu, Zn, Cd, and Pb in seawater using the Nobias-chelate PA1 resin and magnetic sector inductively coupled plasma mass spectrometry (ICP-MS). Marine Chemistry. https://doi.org/10.1016/j.marchem.2011.12.001.

Bown, Johann, Laan, Peter, Ossebaar, Sharyn, Bakker, Karel, Rozema, Patrick, de Baar, Hein J.W., 2017. Bioactive trace metal time series during austral summer in Ryder Bay, Western Antarctic peninsula. Deep Sea Research Part II: Topical Studies in Oceanography 139, 103–119. https://doi.org/10.1016/j.dsr2.2016.07.004.

Boyd, Philip W., Ellwood, Michael J., Tagliabue, Alessandro, Twining, Benjamin S., 2017. Biotic and abiotic retention, recycling and remineralization of metals in the ocean. Nature Geoscience 10, 167–173. https://doi.org/10.1038/ngeo2876.

Brown, Michael S., Munro, David R., Feehan, Colette J., Sweeney, Colm, Ducklow, Hugh W., Schofield, Oscar M., 2019. Enhanced oceanic CO2 uptake along the rapidly changing West Antarctic peninsula. Nature Climate Change 9, 678–683. https://doi.org/10.1038/s41558-019-0552-3.

Bruland, K.W., Middag, R., Lohan, M.C., 2014. Controls of Trace Metals in Seawater. Treatise on Geochemistry (Second Edition). Elsevier, pp. 19–51.

Bucciarelli, Eva, Blain, Stéphane, Tréguer, Paul, 2001. Iron and manganese in the wake of the Kerguelen Islands (Southern Ocean). Marine Chemistry 73, 21–36. https://doi.org/10.1016/S0304-4203(00)00070-0.

Bullard, Joanna E., Baddock, Matthew, Bradwell, Tom, Crusius, John, Darlington, Eleanor, Gaiero, Diego, Gassó, Santiago, Gisladottir, Gudrun, Hodgkins, Richard, McCulloch, Robert, McKenna-Neuman, Cheryl, Mockford, Tom, Stewart, Helena, Thorsteinsson, Throstur, 2016. High-latitude dust in the Earth system. Reviews of Geophysics 54, 447–485. https://doi.org/10.1002/2016RG000518.

Coale, Kenneth H., Johnson, Kenneth S., Fitzwater, Steve S., Gordon, Michael R., Tanner, Sara, Chavez, Francisco P., Ferioli, Laurie, Sakamoto, Carole, Rogers, Paul, Millero, Frank, Steinberd, Paul, Nightingale, Phil, Cooper, David, Cochlan, William P., Landry, Michael R., Constantinou, John, Rollwagen, Gretchen, Trasvina, Armando, Kudela, Raphael, 1996. A massive phytoplankton bloom induced by an ecosystem-scale iron fertilization experiment in the equatorial Pacific Ocean. Nature 383, 495–501. https://doi.org/10.1038/383495a0.

Cook, A.J., Holland, P.R., Meredith, M.P., Murray, T., Luckman, A., Vaughan, D.G., 2016. Ocean forcing of glacier retreat in the western Antarctic peninsula. Science 353, 283–286. https://doi.org/10.1126/science.aae0017.

Couto, Nicole, Martinson, Douglas G., Kohut, John, Schofield, Oscar, 2017. Distribution of Upper Circumpolar Deep Water on the warming continental shelf of the West Antarctic Peninsula. Journal of Geophysical Research Oceans 122, 5306–5315. https://doi.org/10.1002/2017JC012840.

de Baar, Hein J.W., Philip W. Boyd, Kenneth H. Coale, Michael R. Landry, Atsushi Tsuda, Philipp Assmy, Dorothee C. E. Bakker, Yann Bozec, Richard T. Barber, Mark A. Brzezinski, Ken O. Buesseler, Marie Boyé, Peter L. Croot, Frank Gervais, Maxim Y. Gorbunov, Paul J. Harrison, William T. Hiscock, Patrick Laan, Christiane Lancelot, Cliff S. Law, Maurice Levasseur, Adrian Marchetti, Frank J. Millero, Jun Nishioka, Yukihiro Nojiri, Tim van Oijen, Ulf Riebesell, Micha J. A. Rijkenberg, Hiroaki Saito, Shigenobu Takeda, Klaas R. Timmermans, Marcel J. W. Veldhuis, Anya M. Waite, Chi-Shing Wong, 2005. Synthesis of iron fertilization experiments: From the Iron Age in the Age of Enlightenment. J. Geophys. Res. 110. https://doi.org/10.1029/2004JC002601.

de Jong, Jeroen, Véronique Schoemann, Delphine Lannuzel, Peter Croot, Hein de Baar, Jean-Louis Tison, 2012. Natural iron fertilization of the Atlantic sector of the Southern Ocean by continental shelf sources of the Antarctic peninsula. J. Geophys. Res. 117. https://doi.org/10.1029/2011JG001679.

De Jong, J.T.M., Stammerjon, S.E., Ackley, S.F., Tison, J.-L., Mattielli, N., Schoemann, V., 2015. Sources and fluxes of dissolved iron in the Bellingshausen Sea (West Antarctica): the importance of sea ice, icebergs and the continental margin. Mar. Chem. 177, 518–535. https://doi.org/10.1016/j.marchem.2015.08.004.

Death, R., Wadham, J.L., Monteiro, F., Le Brocq, A.M., Tranter, M., Ridgwell, A., Dutkiewicz, S., Raiswell, R., 2014. Antarctic ice sheet fertilises the Southern Ocean. Biogeosciences 11, 2635–2643. https://doi.org/10.5194/bg-11-2635-2014.

Dong, Shenfu, Sprintall, Janet, Gille, Sarah T., Talley, Lynne, 2008. Southern Ocean mixed-layer depth from Argo float profiles. J. Geophys. Res. 113. https://doi.org/10.1029/2006JC004051.

Ducklow, Hugh W., Fraser, William R., Meredith, Michael P., Stammerjohn, Sharon E., Doney, Scott C., Martinson, Douglas G., Sailley, Sévrine F., Schofield, Oscar M., Steinberg, Deborah K., Venables, Hugh J., Amsler, Charles D., 2013. West Antarctic Peninsula: an ice-dependent coastal marine ecosystem in transition. Oceanography 26, 190–203.

Dulaiova, H., Ardelan, M.V., Henderson, P.B., Charette, M.A., 2009. Shelf-derived iron inputs drive biological productivity in the southern Drake Passage. Glob. Biogeochem. Cycles 23. https://doi.org/10.1029/2008GB003406.

Duprat, L., Kanna, N., Janssens, J., Roukaerts, A., Deman, F., Townsend, A.T., Meiners, K. M., van der Merwe, P., Lannuzel, D., 2019. Enhanced Iron Flux to Antarctic Sea ice via Dust Deposition From Ice-Free Coastal Areas. J. Geophys. Res. Oceans 124 (12), 8538–8557. https://doi.org/10.1029/2019JC015221.

Gao, Y., Xu, G., Zhan, J., Zhang, J., Li, W., Lin, Q., Chen, L., Lin, H., 2013. Spatial and particle size distributions of atmospheric dissolvable iron in aerosols and its input to the Southern Ocean and coastal East Antarctica. Journal of Geophysical Research Atmosphere 118, 12,634–12,648. https://doi.org/10.1002/2013JD020367.

Gao, Yuan, Yu, Shun, Sherrell, Robert M., Fan, Songyun, Bu, Kaixuan, Anderson, James R., 2020. Particle-size distributions and solubility of aerosol Iron over the Antarctic peninsula during austral summer. Journal of Geophysical Research Atmosphere 125. https://doi.org/10.1029/2019JD032082.

Gargett, A., Wells, J., Tejada-Martinez, A.E., Grosch, C.E., 2004. Langmuir supercells: a mechanism for sediment resuspension and transport in shallow seas. Science 306, 1925–1928. https://doi.org/10.1126/science.1100849.

Garibotti, Irene A., Vernett, María, Ferrario, Martha E., Smith, Raymond C., Ross, Robin M., Quetin, Langdon B., 2003. Phytoplankton spatial distribution patterns along the western Antarctic peninsula (Southern Ocean). Mar. Ecol. Prog. Ser. 261, 21–39. https://doi.org/10.3354/meps261021.

Gerringa, L.J.A., Laan, P., van Dijken, G.L., van Haren, H., De Baar, H.J.W., Arrigo, K.R., Alderkamp, A.C., 2015. Sources of iron in the Ross Sea Polynya in early summer. Mar. Chem. 177, 447–459. https://doi.org/10.1016/j.marchem.2015.06.002.

Gerringa, L.J.A., Alderkamp, A.C., Laan, P., Thuroczy, C.E., De Baar, H.J.W., Mills, M.M., van Dijken, G.L., van Haren, Hans, Arrigo, K.R., et al., 2012. Iron from melting glaciers fuels the phytoplankton blooms in Amundsen Sea (Southern Ocean): Iron biogeochemistry. Deep Sea Research Part II: Topical Studies in Oceanography 71-76, 16–31. https://doi.org/10.1016/j.dsr2.2012.03.007.

Gerringa, L.J.A., Alderkamp, A.-C., van Dijken, G., Laan, P., Middag, R., Arrigo, K.R., 2020. Dissolved trace metals in the Ross Sea. Front. Marine Sci. 7 https://doi.org/10.3389/fmars.2020.577098.

Grotov, A.S., Nechaev, D.A., Panteleev, G.G., Yaremchuk, M.I., 1998. Large scale circulation in the Bellingshausen and Amundsen seas as a variational inverse of climatological Data. J. Geophys. Res. 103.

Hatta, M., Measures, C.I., Selph, K.E., Zhou, M., Hiscock, W.T., 2013. Iron fluxes from the shelf regions near the South Shetland Islands in the Drake Passage during the austral-winter 2006. Deep Sea Research Part II: Topical Studies in Oceanography 90, 89–101. https://doi.org/10.1016/j.dsr2.2012.11.003.

Henley, S.F., Cavan, E.L., Fawcett, S.E., Kerr, R., Monteiro, T., Sherrell, R.M., Bowie, A. R., Boyd, P.W., Barnes, D.K.A., Schloss, I.R., Marshall, T., Flynn, R., Smith, S., 2020. Changing biogeochemistry of the Southern Ocean and its ecosystem implications. Front. Mar. Sci. 7 https://doi.org/10.3389/fmars.2020.00581.

Hodson, Andy, Nowak, Aga, Sabacka, Marie, Jungblut, Anne, Navarro, Francisco, Pearce, David, Ávila-Jiménez, María Luisa, Convey, Peter, Vieira, Gonçalo, 2017. Climatically sensitive transfer of iron to maritime Antarctic ecosystems by surface runoff. Nature Communications 8. https://doi.org/10.1038/ncomms14499 (2017).

Hofmann, Eileen E., Klinck, John M., Lascara, Cathy M., Smith, David A., 1996. Water mass distribution and circulation west of the Antarctic peninsula and including Bransfield Strait. Antarctic Research Series 70, 61–80. https://doi.org/10.1029/AR070p0061.

Holland, P.R., Brisbourne, A., Corr, H.F.J., McGrath, D., Purdon, K., Paden, J., Fricker, H. A., Paolo, F.S., Fleming, A.H., 2015. Oceanic and atmospheric forcing of Larsen C ice-shelf thinning. The Cryosphere 9, 1005–1024. https://doi.org/10.5194/tc-9-1005-2015.

Holmes, Thomas M., Wuttig, Kathrin, Chase, Zanna, van der Merwe, Pier, Townsend, Ashley T., Schallenberg, Christina, Tonnard, Manon, Bowie, Andrew R., 2019. Iron availability influences nutrient drawdown in the Heard and McDonald Islands region, Southern Ocean. Marine Chemistry 211, 1–14. https://doi.org/10.1016/j.marchem.2019.03.002.

Homoky, William B., John, Seth G., Conway, Tim M., Mills, Rachel A., 2013. Distinct iron isotopic signatures and supply from marine sediment dissolution. Nature Communications volume 4. https://doi.org/10.1038/ncomms3143.

Hoppema, Mario, de Baar, Hein J.W., Bellerby, Richard G.J., Fahrbach, Eberhard, Bakker, Karel, 2002. Annual export production in the interior Weddell Gyre estimated from a chemical mass balance of nutrients. Deep Sea Research Part II: Topical Studies in Oceanography 49, 1675–1689. https://doi.org/10.1016/S0967-0645(02)00006-1.

Hopwood, Mark J., Carroll, Dustin, Höfer, Juan, Achterberg, Eric P., Meire, Lorenz, Le Moigne, Frédéric A.C., Bach, Lennart T., Eich, Charlotte, Sutherland, David A., González, Humberto E., 2019. Highly variable iron content modulates iceberg-ocean fertilisation and potential carbon export. Nature Communications volume 10. https://doi.org/10.1038/s41467-019-13231-0.

Howard, S.L., Hyatt, J., Padman, L., 2004. Mixing in the pycnocline over the western Antarctic peninsula shelf during Southern Ocean GLOBEC. Deep Sea Research Part II: Topical Studies in Oceanography 51, 1965–1979. https://doi.org/10.1016/j.dsr2.2004.08.002.

Johnson, Kenneth S., Michael Gordon, R., Coale, Kenneth H., 1997. What controls dissolved iron concentrations in the world ocean? Marine Chemistry 57, 137–161. https://doi.org/10.1016/S0304-4203(97)00043-1.

Joy-Warren, Hannah L., van Dijken, Gert L., Alderkamp, Anne-Carlijn, Leventer, Amy, Lewis, Kate M., Selz, Virginia, Lowry, Kate E., van de Poll, Willem, Arrigo, Kevin R., 2019. Light is the primary driver of early season phytoplankton production along the Western Antarctic peninsula. Journal of Geophysical Research Oceans 124, 7375–7399. https://doi.org/10.1029/2019JC015295.

Kavanaugh, M.T., Abdala, F.N., Ducklow, H., Glover, D., Fraser, W., Martinson, D., Stammerjohn, S., Schofield, O., Doney, S.C., 2015. Effect of continental shelf canyons on phytoplankton biomass and community composition along the western Antarctic Peninsula. Mar. Ecol. Prog. Ser. 524, 11–26. https://doi.org/10.3354/meps11189.

Klinck, John M., 1998. Heat and salt changes on the continental shelf west of the Antarctic peninsula between January 1993 and January 1994. Journal of Geophysical Research Oceans 103, 7617–7636. https://doi.org/10.1029/98JC00369.

Klinck, J.M., Hofmann, E.E., Beardsley, R.C., Salihoglu, B., Howard, S., et al., 2004. Water-mass properties and circulation on the west Antarctic Peninsula Continental Shelf in Austral Fall and Winter 2001. Deep Sea Research Part II: Topical Studies in Oceanography. https://doi.org/10.1016/j.dsr2.2004.08.001.

Kunz, Matthias, King, Matt A., Mills, Jon P., Miller, Pauline E., Fox, Adrian J., Vaughan, David G., Marsh, Stuart H., 2012. Multi-decadal glacier surface lowering in the Antarctic Peninsula. Geophysical Research Letters 39. https://doi.org/10.1029/2012GL052823.

Lannuzel, Delphine, Schoemann, Véronique, de Jong, Jeroen, Tison, Jean-Louis, Chou, Lei, 2007. Distribution and biogeochemical behaviour of iron in the East Antarctic Sea ice. Marine Chemistry 106, 18–32. https://doi.org/10.1016/j.marchem.2006.06.010.

Lannuzel, Delphine, Schoemann, Véronique, de Jong, Jeroen, Pasquer, Bénédicte, van der Merwe, Pier, Masson, Florence, Tison, Jean-Louis, Bowie, Andrew, 2010. Distribution of dissolved iron in Antarctic Sea ice: spatial, seasonal, and inter-annual variability. Journal of Geophysical Research Biogeosciences 115. https://doi.org/10.1029/2009JG001031.

Lannuzel, Delphine, Bowie, Andrew R., van der Merwe, Pier C., Townsend, Ashley T., Schoemann, Véronique, 2011. Distribution of dissolved and particulate metals in Antarctic Sea ice. Marine Chemistry 124, 134–146. https://doi.org/10.1016/j.marchem.2011.01.004.

Lannuzel, Delphine, van der Merwe, Pier C., Townsend, Ashley T., Bowie, Andrew R., 2014. Size fractionation of iron, manganese and aluminium in Antarctic fast ice reveals a lithogenic origin and low iron solubility. Marine Chemistry 161, 47–56. https://doi.org/10.1016/j.marchem.2014.02.006.

Lin, Hai, Rauschenberg, Sara, Hexel, Cole R., Shaw, Timothy J., Twining, Benjamin S., 2011. Free-drifting icebergs as sources of iron to the Weddell Sea. Deep Sea Research Part II: Topical Studies in Oceanography 58, 1392–1406. https://doi.org/10.1016/j.dsr2.2010.11.020.

Marrari, Maria, Daly, Kendra L., Hu, Chuanmin, et al., 2008. Spatial and temporal variability of SeaWiFS chlorophyll a distributions west of the Antarctic Peninsula: Implications for krill production. Deep Sea Research Part II: Topical Studies in Oceanography 5 (3–4), 377–392. https://doi.org/10.1016/j.dsr2.2007.11.011.

Marshall, Gareth J., Orr, Andrew, van Lipzig, Nicole P.M., King, John C., 2006. The impact of a changing southern hemisphere annular mode on Antarctic Peninsula summer temperatures. Journal of Climate 19, 5388–5404. https://doi.org/10.1175/JCLI3844.1.

Martin, John H., 1990. Glacial-interglacial CO2 change: The Iron Hypothesis. Paleoceanography and Paleoclimatology 5, 1–13. https://doi.org/10.1029/PA005i001p00001.

Martinson, D.G.S., Iannuzzi, Sharon E., Smith, Richard A., Vernet, Raymond C., Maria, 2008. Western Antarctic peninsula physical oceanography and spatio–temporal variability. Deep-Sea Res. II Top. Stud. Oceanogr. 55, 1964–1987.

Martinson, D.G., McKee, D.C., 2012. Transport of warm Upper Circumpolar Deep Water onto the western Antarctic Peninsula continental shelf. Ocean Science 8, 433–442. https://doi.org/10.5194/os-8-433-2012.

Measures, C.I., Brown, M.T., Selph, K.E., Apprill, A., Zhou, M., Hatta, M., Hiscock, W.T., 2013. The influence of shelf processes in delivering dissolved iron to the HNLC waters of the Drake Passage, Antarctica. Deep Sea Research Part II: Topical Studies in Oceanography 90, 77–88. https://doi.org/10.1016/j.dsr2.2012.11.004.

Meredith, Michael P., Brandon, Mark A., Wallace, Maragret I., Clarke, Andrew, Leng, Melanie J., Renfrew, Ian A., van Lipzig, Nicole P.M., King, John C., 2008. Variability in the freshwater balance of northern Marguerite Bay, Antarctic Peninsula: Results from $\delta^{18}O$. Deep Sea Research Part II: Topical Studies in Oceanography 55, 309–322. https://doi.org/10.1016/j.dsr2.2007.11.005.

Meredith, Michael P., Venables, Hugh J., Clarke, Andrew, Ducklow, Hugh W., Erickson, Matthew, Leng, Melanie J., Lenaerts, Jan T.M., van den Broeke, Michiel R., 2013. The freshwater system west of the Antarctic Peninsula: spatial and temporal changes. Journal of Climate 26, 1669–1684. https://doi.org/10.1175/JCLI-D-12-00246.1.

Meredith, Michael P., Stammerjohn, Sharon E., Venables, Hugh J., Ducklow, Hugh W., Martinson, Douglas G., Iannuzzi, Richard A., Leng, Melanie J., van Wessem, Jan Melchior, Reijmer, Carleen H., Barrand, Nicholas E., 2017. Changing distributions of sea ice melt and meteoric water west of the Antarctic Peninsula. Deep Sea Research Part II: Topical Studies in Oceanography 139, 40–57. https://doi.org/10.1016/j.dsr2.2016.04.019.

Millero, Frank J., Sotolongo, Sara, Izaguirre, Miguel, 1987. The oxidation-kinetics of Fe (II) in seawater. Geochimica et Cosmochimica Acta 51, 793–801. https://doi.org/10.1016/0016-7037(87)90093-7.

Moffat, C., Meredith, M., 2018. Shelf-ocean exchange and hydrography west of the Antarctic Peninsula: a review. Philos. Trans. A Math. Phys. Eng. Sci. 376 https://doi.org/10.1098/rsta.2017.0164.

Moffat, Carlos, Beardsley, Robert C., Owens, Breck, van Lipzig, Nicole, 2008. A first description of the Antarctic Peninsula Coastal Current. Deep Sea Research Part II: Topical Studies in Oceanography 55, 277–293. https://doi.org/10.1016/j.dsr2.2007.10.003.

Moffat, C., Owens, B., Beardsley, R.C., 2009. On the characteristics of Circumpolar Deep Water intrusions to the west Antarctic Peninsula Continental Shelf. Journal of Geophysical Research Oceans 114. https://doi.org/10.1029/2008JC004955.

Moore, C.M., Mills, M.M., Arrigo, K.R., Berman-Frank, I. , Bopp, L., Boyd, P.W., Galbraith, E.D., Geider, R.J., Guieu, C., Jaccard, S.L., Jickells, T.D., La Roche, J., Lenton, T.M., Mahowald, N.M., Marañón, E., Marinov, I., Moore, J.K., Nakatsuka, T., Oschlies, A., Saito, M.A., Thingstad, T.F., Tsuda, A., Ulloa, O., 2013. Processes and patterns of oceanic nutrient limitation. Nature Geoscience 6, 701–710. https://doi.org/10.1038/ngeo1765.

Okubo, Akira, 1971. Oceanic diffusion diagrams. Deep-Sea Research 18, 789–802. https://doi.org/10.1016/0011-7471(71)90046-5.

Oliver, Hilde, St-Laurent, Pierre, Sherrell, Robert M., Yager, Patricia L., 2019. Modeling iron and light controls on the summer *Phaeocystis antarctica* bloom in the Amundsen Sea Polynya. Global Biogeochemical Cycles 33, 570–596. https://doi.org/10.1029/2018GB006168.

Parekh, P., Follows, M.J., Boyle, E.A., 2005. Decoupling of iron and phosphate in the global ocean. Global Biogeochemical Cycles 19. https://doi.org/10.1029/2004GB002280.

Planquette, H., Statham, P.J., Fones, G.R., Charette, M.A., Moore, C.M., Salter, I., Nédélec, F.H., Taylor, S.L., French, M., Baker, A.R., Mahowald, N., Jickells, T.D., 2007. Dissolved iron in the vicinity of the Crozet Islands, Southern Ocean. Deep Sea Research Part II: Topical Studies in Oceanography 54, 1999–2019. https://doi.org/10.1016/j.dsr2.2007.06.019.

Prézelin, B.B., Hofmann, E.E., Moline, M., Klinck, J.M., 2004. Physical forcing of phytoplankton community structure and primary production in continental shelf waters of the Western Antarctic Peninsula. Journal of Marine Research 62, 419–460. https://doi.org/10.1357/0022240041446173.

Pritchard, H.D., Vaughan, D.G., 2007. Widespread acceleration of tidewater glaciers on the Antarctic Peninsula. Journal of Geophysical Research Earth Surface 112. https://doi.org/10.1029/2006JF000597.

Rafter, Patrick A., Sigman, Daniel M., Mackey, Katherine R.M., 2017. Recycled iron fuels new production in the eastern equatorial Pacific Ocean. Nature Communications 8. https://doi.org/10.1038/s41467-017-01219-7.

Raiswell, Rob, Benning, Lianne G., Tranter, Martyn, Tulaczyk, Slawek, 2008. Bioavailable iron in the Southern Ocean: the significance of the iceberg conveyor belt. Geochemical Transactions 9. https://doi.org/10.1186/1467-4866-9-7.

Raiswell, Robert, Hawkings, Jon R., Benning, Liane G., Baker, Alex R., Death, Ros, Albani, Samuel, Mahowald, Natalie, Krom, Michael D., Poulton, Simon W., Wadham, Jemma, Tranter, Martyn, 2016. Potentially bioavailable iron delivery by iceberg-hosted sediments and atmospheric dust to the polar oceans. Biogeosciences 13, 3887–3900. https://doi.org/10.5194/bg-13-3887-2016.

Randall-Goodwin, E., Meredith, M.P., Jenkins, A., Yager, P.L., Sherrell, R.M., Abrahamsen, E.P., Guerrero, R., Yuan, X., Mortlock, R.A., Gavahan, K., Alderkamp, A.C., Ducklow, H., Robertson, R., Stammerjohn, S.E., 2015. Freshwater distributions and water mass structure in the Amundsen Sea Polynya region, Antarctica. Elementa: Science of the Anthropocene 3. https://doi.org/10.12952/journal.elementa.000065.

Raven, John A., 1988. The Iron and molybdenum use efficiencies of plant-growth with different energy, carbon and nitrogen-sources. New Phytologist 109, 279–287. https://doi.org/10.1111/j.1469-8137.1988.tb04196.x.

Richon, C., Aumont, O., Tagliabue, A., 2020. Prey stoichiometry drives iron recycling by zooplankton in the Global Ocean. Frontiers in Marine Science 7. https://doi.org/10.3389/fmars.2020.00451.

Sarmiento, J.L., Slater, R., Barber, R., Bopp, L., Doney, S.C., Hirst, A.C., Kleypas, J., Matear, R., Mikolajewicz, U., Monfray, P., Soldatov, V., Spall, S.A., Stouffer, R., 2004. Response of ocean ecosystems to climate warming. Global Biogeochemical Cycles 18. https://doi.org/10.1029/2003GB002134.

Savidge, Dana K., Amft, Julie A., 2009. Circulation on the West Antarctic Peninsula derived from 6 years of shipboard ADCP transects. Deep Sea Research Part I: Oceanographic Research Papers 56, 1633–1655. https://doi.org/10.1016/j.dsr.2009.05.011.

Schallenberg, Christina, van der Merwe, Pier, Chever, Fanny, Cullen, Jay T., Lannuzel, Delphine, Bowie, Andrew R., 2016. Dissolved iron and iron(II) distributions beneath the pack ice in the East Antarctic (120°E) during the winter/spring transition. Deep Sea Research Part II: Topical Studies in Oceanography 131, 96–110. https://doi.org/10.1016/j.dsr2.2015.02.019.

Schofield, Oscar, Ducklow, Hugh, Bernard, Kim, Doney, Scott, Patterson-Fraser, Donna, Gorman, Kristen, Martinson, Doug, Meredith, Michael, Saba, Grace, Stammerjohn, Sharon, Steinberg, Deborah, Fraser, William, 2013. Penguin biogeography along the West Antarctic Peninsula: testing the canyon hypothesis with Palmer LTER Observations. Oceanography 26, 204–206. https://www.jstor.org/stable/24862082.

Sedwick, P.N., Marsay, C.M., Sohst, B.M., Aguilar-Islas, A.M., Lohan, M.C., Long, M.C., Arrigo, K.R., Dunbar, R.B., Saito, M.A., Smith, W.O., DiTullio, G.R., 2011. Early

season depletion of dissolved iron in the Ross Sea polynya: implications for iron dynamics on the Antarctic continental shelf. Journal of Geophysical Research Oceans 116. https://doi.org/10.1029/2010JC006553.

Sherman, J., Gorbunov, M.Y., Schofield, O., Falkowski, P.G., 2020. Photosynthetic energy conversion efficiency in the West Antarctic Peninsula. Limnol. Oceanogr. 65, 2912–2925. https://doi.org/10.1002/lno.11562.

Sherrell, Robert M., Annett, Amber L., Fitzsimmons, Jessica N., Roccanova, Vincent J., Meredith, Michael P., 2018. A 'shallow bathtub ring' of local sedimentary iron input maintains the Palmer Deep biological hotspot on the West Antarctic Peninsula shelf. Phil. Trans. R. Soc. A. 376 https://doi.org/10.1098/rsta.2017.0171.

Sieber, M., Conway, T.M., de Souza, G.F., Hassler, C.S., Ellwood, M.J., Vance, D., 2021. Isotopic fingerprinting of biogeochemical processes and iron sources in the iron-limited surface Southern Ocean. Earth and Planetary Science Letters 567, 1–12. https://doi.org/10.1016/j.epsl.2021.116967, 116967.

Smith, D.A., Hofmann, E.E., Klinck, J.M., Lascara, C.M., 1999. Hydrography and circulation of the West Antarctic Peninsula continental shelf. Deep Sea Research Part I: Oceanographic Research Papers 46, 925–949. https://doi.org/10.1016/S0967-0637(98)00103-4.

Smith, Raymond C., Martinson, Douglas G., Stammerjohn, Sharon E., Iannuzzi, Richard A., Ireson, Kirk, 2008. Bellingshausen and western Antarctic Peninsula region: pigment biomass and sea-ice spatial/temporal distributions and interannual variabilty. Deep Sea Research Part II: Topical Studies in Oceanography 55, 1949–1963. https://doi.org/10.1016/j.dsr2.2008.04.027.

St-Laurent, P., Yager, P.L., Sherrell, R.M., Stammerjohn, S.E., Dinniman, M.S., 2017. Pathways and supply of dissolved iron in the Amundsen Sea (Antarctica). Journal Geophysical Research Oceans 122, 7135–7162. https://doi.org/10.1002/2017JC013162.

Steinberg, Deborah K., Martinson, Douglas G., Costa, Daniel P., 2012. Two decades of pelagic ecology of the Western Antarctic Peninsula. Oceanography 25, 56–67. http://www.jstor.org/stable/24861394.

St-Laurent, P., Yager, P.L., Sherrell, R.M., Oliver, H., Dinniman, M.S., Stammerjohn, S.E., 2019. Modeling the seasonal cycle of Iron and carbon fluxes in the Amundsen Sea Polynya, Antarctica. Journal Geophysical Research Oceans 124, 1544–1565. https://doi.org/10.1029/2018JC014773.

Tagliabue, Alessandro, Bopp, Laurent, Dutay, Jean-Claude, Bowie, Andrew R., Chever, Fanny, Jean-Baptiste, Philippe, Bucciarelli, Eva, Lannuzel, Delphine, Remenyi, Thomas, Sarthou, Géraldine, Aumont, Olivier, Gehlen, Marion, Jeandel, Catherine, 2010. Hydrothermal contribution to the oceanic dissolved iron inventory. Nature Geoscience 3, 252–256. https://doi.org/10.1038/ngeo818.

Tagliabue, Alessandro, Bopp, Laurent, Aumont, Olivier, 2009. Evaluating the importance of atmospheric and sedimentary iron sources to Southern Ocean biogeochemistry. Geophysical Research Letters 36. https://doi.org/10.1029/2009GL038914.

Tagliabue, Alessandro, Sallée, Jean-Baptiste, Bowie, Andrew R., Lévy, Marina, Swart, Sebastian, Boyd, Philip W., 2014. Surface-water iron supplies in the Southern Ocean sustained by deep winter mixing. Nature Geoscience 7, 314–320. https://doi.org/10.1038/ngeo2101.

Tagliabue, Alessandro, Bowie, Andrew R., Boyd, Philip W., Buck, Kristen N., Johnson, Kenneth S., Saito, Mak A., 2017. The integral role of iron in ocean biogeochemistry. Nature 543, 51–59. https://doi.org/10.1038/nature21058.

Twelves, A.G., Goldberg, D.N., Henley, S.F., Mazloff, M.R., Jones, D.C., 2021. Self-shading and meltwater spreading control the transition from light to iron limitation in an Antarctic coastal polynya. Journal of Geophysical Research Oceans 126. https://doi.org/10.1029/2020JC016636.

Twining, Benjamin S., Baines, Stephen B., 2013. The trace metal composition of marine phytoplankton. Annu. Rev. Mar. Sci. 5, 191–215. https://doi.org/10.1146/annurev-marine-121211-172322.

Twining, Benjamin S., Baines, Stephen B., Fischer, Nicholas S., Landry, Michael R., 2004. Cellular iron contents of plankton during the Southern Ocean Iron Experiment (SOFeX). Deep Sea Research Part I: Oceanographic Research Papers 51, 1827–1850. https://doi.org/10.1016/j.dsr.2004.08.007.

van der Merwe, P., Lannuzel, D., Bowie, A.R., Meiners, K.M., 2011. High temporal resolution observations of spring fast ice melt and seawater iron enrichment in East Antarctica. Journal of Geophysical Research Biogeosciences 116. https://doi.org/10.1029/2010JG001628.

van Haren, Hans, Brussaard, Corina P.D., Gerringa, Loes J.A., van Manen, Mathijs H., Middag, Rob, Groenewegen, Ruud, 2021. Diapycnal mixing across the photic zone of the NE Atlantic. Ocean Science 17, 301–318. https://doi.org/10.5194/os-17-301-2021.

van Leeuwe, Maria A., Webb, Alison L., Venables, Hugh J., Visser, Ronald J.W., Meredith, Mike P., M. Elzenga, J. Theo, Stefels, Jacqueline, 2020. Annual patterns in phytoplankton phenology in Antarctic coastal waters explained by environmental drivers. Limnology and Oceanography 65, 1651–1668. https://doi.org/10.1002/lno.11477.

van Wessem, J.M., Meredith, M.P., Reijmer, C.H., van den Broeke, M.R., Cook, A.J., 2017. Characteristics of the modelled meteoric freshwater budget of the western Antarctic Peninsula. Deep Sea Research Part II: Topical Studies in Oceanography 139, 31–39. https://doi.org/10.1016/j.dsr2.2016.11.001.

Venables, Hugh J., Meredith, Michael P., Alexander Brearley, J., 2017. Modification of deep waters in Marguerite Bay, western Antarctic peninsula, caused by topographic overflows. Deep Sea Research Part II: Topical Studies in Oceanography 139, 9–17. https://doi.org/10.1016/j.dsr2.2016.09.005.

Vernet, Maria, Martinson, Douglas, Iannuzzi, Richard, Stammerjohn, Sharon, Kozlowski, Wendy, Sines, Karie, Smith, Ray, Garibotti, Irene, 2008. Primary production within the sea-ice zone west of the Antarctic peninsula: I—Sea ice, summer mixed layer, and irradiance. Deep Sea Research Part II: Topical Studies in Oceanography 55, 2068–2085. https://doi.org/10.1016/j.dsr2.2008.05.021.

Wadham, J.L., Death, R., Monteiro, F.M., Tranter, M., Ridgwell, A., Raiswell, R., Tulaczyk, S., 2013. The potential role of the Antarctic ice sheet in global biogeochemical cycles. Earth and Environmental Science Transactions of the Royal Society of Edinburgh 104, 55–67. https://doi.org/10.1017/S1755691013000108.

Williams, G.D., Meijers, A.J.S., Poole, A., Mathiot, P., Tamura, T., Klocker, A., 2011. Late winter oceanography off the Sabrina and BANZARE coast (117–128°E), East Antarctica. Deep Sea Research Part II: Topical Studies in Oceanography 58, 1194–1210. https://doi.org/10.1016/j.dsr2.2010.10.035.

Winton, V.H.L., Bowie, A.R., Edwards, R., Keywood, M., Townsend, A.T., van der Merwe, P., Bollhöfer, A., et al., 2015. Fractional iron solubility of atmospheric iron inputs to the Southern Ocean. Marine Chemistry 177, 20–32. https://doi.org/10.1016/j.marchem.2015.06.006.

Yang, Bo, Shadwick, Elizabeth H., Schultz, Christina, Doney, Scott C., 2021. Annual mixed layer carbon budget for the West Antarctic Peninsula continental shelf: insights from year-round mooring measurements. Journal of Geophysical Research Oceans 126. https://doi.org/10.1029/2020JC016920.